Nonlinear double-diffusive convection

By HERBERT E. HUPPERT AND DANIEL R. MOORE

Department of Applied Mathematics and Theoretical Physics,
University of Cambridge

The two-dimensional motion of a fluid confined between two long horizontal planes, heated and salted from below, is examined. By a combination of perturbation analysis and direct numerical solution of the governing equations, the possible forms of large-amplitude motion are traced out as a function of the four non-dimensional parameters which specify the problem: the thermal Rayleigh number R_T, the saline Rayleigh number R_S, the Prandtl number σ and the ratio of the diffusivities τ. A branch of time-dependent asymptotic solutions is found which bifurcates from the linear oscillatory instability point. In general, for fixed σ, τ and R_S, as R_T increases three further abrupt transitions in the form of motion are found to take place independent of the initial conditions. At the first transition, a rather simple oscillatory motion changes into a more complicated one with different structure, at the second, the motion becomes aperiodic and, at the third, the only asymptotic solutions are time independent. Disordered motions are thus suppressed by increasing R_T. The time-independent solutions exist on a branch which, it is conjectured, bifurcates from the time-independent linear instability point. They can occur for values of R_T less than that at which the third transition point occurs. Hence for some parameter ranges two different solutions exist and a hysteresis effect occurs if solutions obtained by increasing R_T and then decreasing R_T are followed. The minimum value of R_T for which time-independent motion can occur is calculated for fourteen different values of σ, τ and R_S. This minimum value is generally much less than the critical value of time-independent linear theory and for the larger values of σ and R_S and the smaller values of τ, is less than the critical value of time-dependent linear theory.

1. Introduction

Since its birth as 'an oceanographical curiosity' (Stommel, Arons & Blanchard 1956), double-diffusive convection has matured into a subject with a large variety of applications. Many situations exist in oceanography, astrophysics and chemical engineering, to cite only three areas, where there are two components of different molecular diffusivities which contribute in an opposing sense to the vertical density gradient. Whether the components are heat and salt, as in the oceanographic situation, heat and helium, as in the astrophysical situation, or two different solutes, as in chemical engineering situations, the qualitative

aspects of double-diffusive convection are the same; only the time and possibly space scales of the motion are different. In addition to the many applications, interest in the subject has developed as a result of the marked difference between double-diffusive convection and convection involving only one component, as for example in purely thermal convection. In contrast to thermal convection, motions can arise even when the density decreases with height, that is, when the basic state is statically stable. This is due to the effects of diffusion, which is a stabilizing influence in thermal convection, but can act in a double-diffusive fluid in such a way as to release potential energy stored in one of the components, and convert it into the kinetic energy of the motion.

The physical mechanism underlying one of the fundamental forms of double-diffusive motion can be understood from the following parcel argument. Using the terminology of heat and salt, as we shall throughout this paper, consider a fluid whose temperature, salinity and density all decrease monotonically with height. If a fluid parcel is raised it comes into a cooler, less salty and less dense environment. Because the rate of molecular diffusion of heat is larger than that of salt, the thermal field of the parcel tends to equilibrate with its surroundings more rapidly than does the salt field. The parcel is then heavier than its surroundings and sinks. But owing to the finite value of the thermal diffusion coefficient, the temperature field of the parcel lags the displacement field and the parcel returns to its original position heavier than it was at the outset. It then sinks to a depth greater than the original rise, whereupon the above process continues, leading to growing oscillations, or overstability as it is sometimes called, which is resisted only by the effects of viscosity. This linear mechanism was first explained by Stern (1960)† and explored further in a beautifully written paper (Moore & Spiegel 1966) which develops an analogy between this form of double-diffusive convection and the motion of a flaccid balloon in a thermally stratified fluid. If the temperature gradient is sufficiently large compared with the salinity gradient, nonlinear disturbances may exist which lead to time-independent motion because the large temperature field is then able to overcome the restoring tendency of the salinity field.

An evaluation of the conditions under which this time-independent form of motion can occur is one of the aims of this paper. One of the important aspects of time-independent motion is that the heat and salt transports are very much larger than those in typical time-dependent motions. Thus an evolution calculation for a laboratory experiment, an oceanographical situation or a star will be significantly dependent upon what form of double-diffusive motions exists.

The traditional geometry in which convective motions have been quantitatively analysed confines the fluid between two infinite horizontal planes, heated, and in our case also salted, from below. In the purely thermal situation, many of the theoretically determined results have been experimentally verified and successfully used to explain various phenomena, as summarized by Spiegel (1971). In a double-diffusive situation, using this geometry, Huppert & Manins (1973) develop some theoretical results which accurately predict the outcome

† In a footnote.

of a series of experiments in which two deep uniform layers of different solute concentrations were initially separated by a paper-thin horizontal interface. For details the reader is referred to the original paper. The essential comment to be made here is that the theoretical model, which incorporates the seemingly constraining presence of the horizontal planes, was successfully used in a situation uninfluenced by boundaries.

Turning now to an explicit statement of the model analysed in this paper, we consider a fluid which occupies the space between two infinite horizontal planes separated by a distance D. The upper plane is maintained at temperature T_0 and salinity S_0 and the lower plane at temperature $T_0 + \Delta T$ and salinity $S_0 + \Delta S$. Both planes are assumed to be stress free and perfect conductors of heat and salt. We restrict attention to two-dimensional motion, dependent only upon one horizontal co-ordinate and the vertical co-ordinate, and discuss in §7 the consequences of this restriction. We non-dimensionalize all lengths with respect to D and time with respect to D^2/κ_T, where κ_T is the thermal diffusivity, and express the velocity $\mathbf{q}^*$ in terms of a stream function ψ by

$$\mathbf{q}^* = (\kappa_T/D)\,(\psi_z, -\psi_x), \tag{1.1}$$

the temperature T^* by

$$T^* = T_0 + \Delta T(1 - z + T) \tag{1.2}$$

and the salinity S^* by

$$S^* = S_0 + \Delta S(1 - z + S), \tag{1.3}$$

so that we can write the governing Boussinesq equations of motion as

$$\sigma^{-1}\nabla^2\partial_t\psi - \sigma^{-1}J(\psi, \nabla^2\psi) = -R_T\,\partial_x T + R_S\,\partial_x S + \nabla^4\psi, \tag{1.4}$$

$$\partial_t T + \partial_x\psi - J(\psi, T) = \nabla^2 T, \tag{1.5}$$

$$\partial_t S + \partial_x\psi - J(\psi, S) = \tau\nabla^2 S, \tag{1.6}$$

$$\psi = \partial_{zz}^2\psi = T = S = 0 \quad (z = 0, 1), \tag{1.7}$$

where the Jacobian J is defined by

$$J(f, g) = \partial_x f\,\partial_z g - \partial_z f\,\partial_x g. \tag{1.8}$$

We have assumed the linear equation of state

$$\rho^* = \rho_0(1 - \alpha T^* + \beta S^*), \tag{1.9}$$

where α and β are taken to be constant, in the expressions for the body-force term of (1.4).

Four non-dimensional parameters appear in (1.4)–(1.6): the Prandtl number

$$\sigma = \nu/\kappa_T, \tag{1.10}$$

where ν is the kinematic viscosity; the ratio of the diffusivities

$$\tau = \kappa_S/\kappa_T, \tag{1.11}$$

where κ_S is the saline diffusivity, which is less than κ_T; the thermal Rayleigh number

$$R_T = \alpha g\Delta T D^3/(\kappa_T\,\nu), \tag{1.12}$$

where g is gravity; and the saline Rayleigh number

$$R_S = \beta g \Delta S D^3 / (\kappa_T \nu). \tag{1.13}$$

The first two parameters characterize the fluid, while the last two characterize externally applied parameters of the model. In this paper both Rayleigh numbers are positive.† For brevity, we refer to the system (1.4)–(1.7) as $\mathscr{S}_t$.

Some solutions of $\mathscr{S}_t$ were obtained by Veronis (1965, 1968b) in terms of truncated Fourier expansions. He concluded from the latter, more accurate, study that, for $\sigma \geqslant 1$, as R_T is increased oscillatory motion first occurs and then at a value of R_T greater than R_S the motion becomes steady. Veronis conjectured that, for increasingly large values of R_S, the minimum value of R_T for which steady convection can occur tends to R_S. The approach adopted in this paper is very different in both numerical detail and interpretation. The numerical methods employed are supported by analytical calculations which allow a larger range of values of σ, τ and R_S to be investigated. We find that as R_T is increased from zero, steady motion can occur first, at a value of R_T significantly less than R_S.

The linear solutions of $\mathscr{S}_t$ are discussed in § 2. It is shown that the stability boundary occurs at the same horizontal wavelength for both oscillatory and steady linear modes and the possible forms of linear motion are mapped out in an R_T, R_S plane (figure 1).

The horizontal scale of linear theory is then used in the nonlinear investigations discussed in §§ 3–7. Results obtained using different horizontal scales are similar, as briefly discussed in the footnote on page 828. We focus on the asymptotic solutions of $\mathscr{S}_t$, that is those solutions which result from long-time integrations of $\mathscr{S}_t$ considered as an initial-value problem. We find that these solutions may be oscillatory, aperiodic or steady. Further, there exist ranges of σ, τ and R_T for which two stable equilibrium solutions of different character exist. These results are obtained from the combined use of modified perturbation theory (as described for example in Sattinger 1973), direct numerical integration of $\mathscr{S}_t$ and the generally known results concerning solutions of nonlinear differential equations.

From modified perturbation theory, the analytic form of the equilibrium solutions in the vicinity of the linear modes can be investigated by an ordered expansion about these modes. As the degree of nonlinearity increases, the form of solution is numerically investigated by integrating $\mathscr{S}_t$ using finite-difference techniques. The numerical program places constraints on the values of σ and τ for which quantitative results can be obtained. In particular, it is not possible to use the program with $\sigma = 7$ and $\tau = \frac{1}{80}$, the appropriate values for heat and salt in water. However, a sufficient number of different values of σ and τ are investigated to discern the overall pattern of the results. Because it is this

---

† If both Rayleigh numbers are negative the analysis models a fluid in which temperature and salinity increase monotonically with height. In this situation the motion is generally time independent and is due to fluid parcels with downward motion diffusing heat to adjacent rising fluid parcels, much in the manner of a heat exchanger. This form of motion, called salt-fingering, was first explicitly discussed by Stern (1960) and some nonlinear aspects have been considered by Straus (1972).

overall pattern which is of greatest interest, the discussion of the possible forms of solution is fairly general, with the calculated results being used only as quantitative illustrations.

2. Infinitesimal motions

The results of linearized theory have been derived elsewhere (Stern 1960; Veronis 1965, 1968b; Baines & Gill 1969). However, since these results act as a foundation for the nonlinear aspects of our investigations, we restate them briefly in this section in a manner convenient for future reference.

The equations governing infinitesimal motions are obtained by deleting the nonlinear Jacobian terms of (1.4)–(1.6). The resulting differential system has constant coefficients and a solution in terms of the lowest normal modes

$$\left.\begin{aligned} \psi(x,z,t) \\ T(x,z,t) \\ S(x,z,t) \end{aligned}\right\} = \left.\begin{aligned} \psi_0 \sin \pi \alpha x \\ T_0 \cos \pi \alpha x \\ S_0 \cos \pi \alpha x \end{aligned}\right\} e^{pt} \sin \pi z \qquad \begin{aligned} &(2.1a)\\ &(2.1b)\\ &(2.1c) \end{aligned}$$

leads to the dispersion relationship

$$p^3 + (\sigma + \tau + 1)\,k^2 p^2 + [(\sigma + \tau + \sigma\tau)\,k^4 - \pi^2 \sigma \alpha^2 k^{-2}(R_T - R_S)]\,p$$
$$+ \sigma\tau k^6 + \pi^2 \sigma \alpha^2 (R_S - \tau R_T) = 0, \quad (2.2)$$

where
$$k^2 = \pi^2(1 + \alpha^2). \qquad (2.3)$$

Since (2.2) is a cubic with real coefficients its zeros are either all real or consist of one real root and two complex-conjugate roots. Overstability, which arises when the pair of complex-conjugate roots crosses the imaginary axis, $p_r = 0$, occurs when

$$R_T(\alpha) = \frac{\sigma + \tau}{\sigma + 1} R_S + (1 + \tau)(1 + \tau\sigma^{-1})\,k^6/(\pi^2 \alpha^2) \qquad (2.4)$$

and

$$p_i^2 = (\sigma\tau + \sigma + \tau)\,k^4 - \sigma(R_T - R_S)\,\pi^2 \alpha^2 k^{-2}. \qquad (2.5)$$

For fixed values of σ and τ, $R_T(\alpha)$ is least for $\alpha = 2^{-\frac{1}{2}}$, at which value

$$k^6/(\pi^2 \alpha^2) = \tfrac{27}{4}\pi^4, \qquad (2.6a)$$

$$R_T(2^{-\frac{1}{2}}) = \frac{\sigma + \tau}{\sigma + 1} R_S + \tfrac{27}{4}\pi^4(1 + \tau)(1 + \tau\sigma^{-1}) \equiv R_1 \qquad (2.6b)$$

and $p = \pm i p_0$, say. Exchange of stabilities, which arises when one of the roots equals zero, i.e. $p \equiv 0$, or equivalently $\partial_t \equiv 0$, occurs when

$$R_T(\alpha) = R_S/\tau + k^6/(\pi^2 \alpha^2). \qquad (2.7)$$

As before, $R_T(\alpha)$ is least for $\alpha = 2^{-\frac{1}{2}}$, at which value we denote R_T by

$$R_6 = R_S/\tau + \tfrac{27}{4}\pi^4, \qquad (2.8)$$

where the subscript 6 anticipates the development in subsequent sections. Descriptions of and, where possible, analytic expressions for $R_1, \dots, R_6$ are given in table 1.
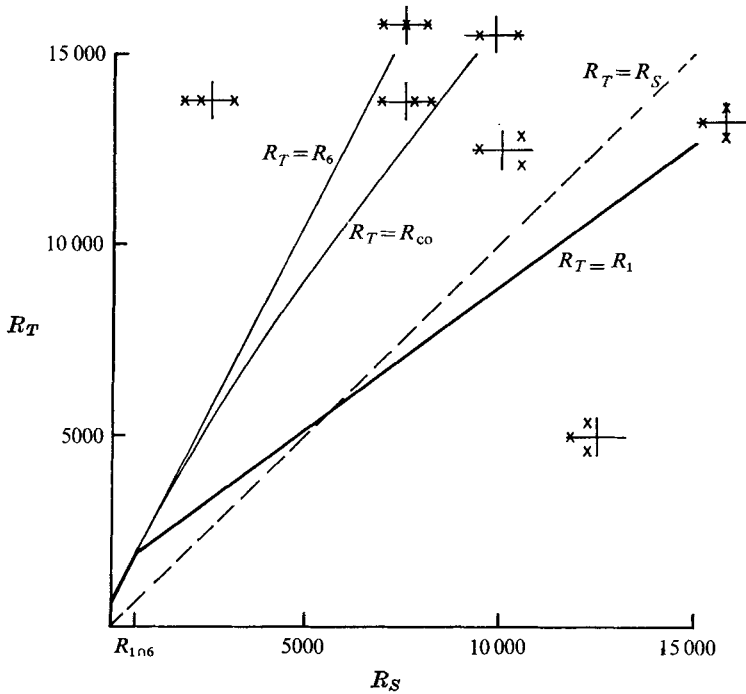
FIGURE 1. The results of linear stability theory for $\sigma = 1\cdot0$, $\tau = 0\cdot5$. Only the region below the two heavy lines is stable to linear disturbances. Each small pair of axes with its three crosses represents the complex p plane and the relative position of the solutions of (2.2) for the values of R_T and R_S at the origin of the axes.

In the R_S, R_T plane the linear stability boundary is a combination of $R_T = R_1$ and $R_T = R_6$, as depicted in figure 1, which presents a complete summary of the linear results for $\sigma = 1$ and $\tau = 0\cdot5$. For $R_S > R_{1n6}$, where

$$R_{1n6} = \tfrac{27}{4}\pi^4\tau^2(1 + \sigma^{-1})\,(1 - \tau)^{-1} \tag{2.9}$$

is the value of R_S at which $R_1 = R_6$, as R_T exceeds R_1 the conduction state is unstable to an oscillatory mode. This instability occurs because of the physical mechanism discussed in the second paragraph of the introduction. For

$$0 < R_S < R_{1n6},$$

the salt gradient is too small for the mechanism which gives rise to the oscillations to be effective and the conduction state is destabilized by a monotonic mode as R_T exceeds R_6.

For fixed $R_S > R_{1n6}$, as R_T increases above R_1, the two complex-conjugate roots acquire positive real parts until $R_T = R_{co}$, say, at which point these roots coalesce on the real axis. The value of R_{co} can be determined from the implicit relationship

$$\left[\tau + \sigma + \sigma\tau + \frac{4\sigma}{27\pi^4}(R_S - R_{co}) - \tfrac{1}{3}(\sigma + \tau + 1)^2\right]^3 + \tfrac{3}{4}\left\{\tfrac{2}{9}(\sigma + \tau + 1)^3\right.$$

$$\left. - (\sigma + \tau + 1)\left(\tau + \sigma + \sigma\tau + \frac{4\sigma}{27\pi^4}(R_S - R_{co})\right) + 3\sigma\left[\tau + \frac{4}{27\pi^4}(R_S - \tau R_{co})\right]\right\}^2 = 0, \tag{2.10}$$

which expresses the condition that (2.2) has a repeated root. The graph of R_{co} as a function of R_S for $\sigma = 1\cdot0$ and $\tau = 0\cdot5$ is presented in figure 1. As R_T increases above R_{co}, one of these two real roots increases and the other decreases until at $R_T = R_6$ the latter root is identically zero. Thus at this exchange-of-stability point, as R_T increases, one root of (2.2) *decreases* through zero, while one of the other roots remains positive, the other negative. For $0 < R_S < R_{1n6}$ there is one positive (real) root and two negative roots for all $R_T > R_6$. Also drawn in figure 1 is the line $R_T = R_S$, above which the basic density is statically unstable.

In summary, the conduction solution bifurcates at $R_T = R_1$ into a pair of conjugate oscillatory solutions and, at $R_T = R_6$, into a monotonic convective solution, where the term monotonic in this paper is synonymous with non-oscillatory. According to linear theory, for $0 < R_S \leqslant R_{1n6}$ convection is always monotonic, while for $R_S > R_{1n6}$ it is oscillatory for $R_1 < R_T < R_{co}$ and monotonic for $R_T \geqslant R_{co}$. Since $R_{co} > R_S$, linear monotonic convection is possible only if the basic density is statically unstable.

Higher normal modes of the form

$$\left.\begin{array}{c} \psi(x,z,t) \\ T(x,z,t) \\ S(x,z,t) \end{array}\right\} = \left.\begin{array}{c} \psi_0 \sin m\pi\alpha x \\ T_0 \cos m\pi\alpha x \\ S_0 \cos m\pi\alpha x \end{array}\right\} e^{pt} \sin n\pi z$$

$$(2.11a)$$
$$(2.11b)$$
$$(2.11c)$$

have critical thermal Rayleigh numbers which can be calculated in the same manner as described above. As before, the lowest values occur for $\alpha = 2^{-\frac{1}{2}}$. Overstability for the (m, n) mode (using obvious notation) sets in at a thermal Rayleigh number given by

$$R_1^{mn} = \frac{\sigma + \tau}{\sigma + 1} R_S + 2\pi^4 m^{-2}(1 + \tau)(1 + \tau\sigma^{-1})(n^2 + \tfrac{1}{2}m^2)^3 \qquad (2.12)$$

and exchange of stabilities at a thermal Rayleigh number given by

$$R_6^{mn} = R_S/\tau + 2\pi^4 m^{-2}(n^2 + \tfrac{1}{2}m^2)^3. \qquad (2.13)$$

The $(2,1)$ modes, with half the horizontal scale of the lowest normal modes, have smaller critical Rayleigh numbers than the $(1, 2)$ modes, with half the vertical scale of the lowest normal modes. These higher modes play no essential part in our investigation and are mentioned here mainly for completeness.

3. Finite-amplitude motions

The main aim of this paper is to examine how the various instability regions of the previous section extend into the nonlinear domain and in particular to determine the possible asymptotic solutions for given R_T and R_S. Essentially, this requires the addition to figure 1 of a third dimension representing the amplitude of the motion. For convenience, graphical results are presented by considering planes of constant R_S, and asymptotic solutions are hence plotted in an R_T, amplitude plane.

Solutions are obtained by direct numerical integration of $\mathscr{S}_t$, supplemented by analytical calculations using modified perturbation techniques. The numerical computation is accomplished by approximating $\mathscr{S}_t$ by space- and time-centred second-order difference equations in ψ, $\nabla^2\psi$, T and S on a rectangular staggered mesh in the domain $0 \leqslant x \leqslant \alpha^{-1} \equiv 2^{\frac{1}{2}}$ and $0 \leqslant z \leqslant 1$. The equations incorporate the periodicity conditions $\psi = \psi_{xx} = T_x = S_x = 0$ at $x = 0$ and α^{-1}. From the equations, values of $\nabla^2\psi$, T and S at the grid points are advanced in time steps of δt. The variable ψ is then calculated from $\nabla^2\psi$ by inverting the Laplacian using an implicit finite-difference approximation to Poisson's equation. This process is repeated for as many time steps as required. The program is an extension of one used originally by Moore, Peckover & Weiss (1973) and is discussed further in the appendix. The appendix also contains a list of almost all the numerical experiments conducted.

A full investigation has been carried out for the 14 sets of (σ, τ, R_S) values displayed in table 3. For each set of parameters, the branch of nonlinear asymptotic solutions emanating from the oscillatory bifurcation point R_1 and the branch of monotonic solutions, presumably emanating from the bifurcation point R_6, are traced out in an R_T, amplitude plane. In particular, the value of R_T below which a monotonic solution cannot exist is found (table 3, column 6).

The amplitude of any solution could be characterized in a number of different ways, using either local values, such as the velocity or stream function at a particular point, or global values, such as the heat or salt transport, or the kinetic energy. In this paper we find it most convenient to use the horizontally averaged heat and salt transport, or their non-dimensional representation, the thermal and saline Nusselt numbers. These are given by

$$N_T(z) = 1 - \overline{\partial_z T} + \overline{wT}, \quad N_S(z) = 1 - \overline{\partial_z S} + \overline{wS}, \qquad (3.1), (3.2)$$

where w is the (non-dimensional) vertical velocity and an overbar denotes a horizontal average. At either of the boundaries $w = 0$ and the second term of (3.1) and (3.2), which is the direct contribution made to the heat transfer by convection, is zero. In particular, at the lower boundary the Nusselt numbers are given by

$$N_T = 1 - \overline{\partial_z T}|_{z=0}, \quad N_S = 1 - \overline{\partial_z S}|_{z=0}, \qquad (3.3), (3.4)$$

where the value at $z = 0$ in the representations on the left-hand side is understood. We use either of these two, or where appropriate their maxima, M_T and M_S, say, as an indication of the amplitude of the motion.

Using a global energy analysis Shir & Joseph (1968) show that for $R_S \geqslant 0$ a *sufficient* condition for the conduction solution to be the only solution of $\mathscr{S}_t$ is that $R_T < \frac{27}{4}\pi^4$. However, we find that for all of the parameter space which we investigate, the conduction solution is the only solution for a range of values of R_T larger than $\frac{27}{4}\pi^4$. The double-diffusive Bénard problem heated and salted below hence provides an example where straightforward global analysis does not yield attained bounds.† This result should be contrasted with the case of negative

† This conclusion is based on the additional facts that the solutions outlined in this paper for $\alpha = 2^{-\frac{1}{2}}$ are relatively insensitive to a change in α to within a factor of 2, and, in particular, that the minimum value of R_T for which convection can be sustained at $\alpha = 2^{-\frac{1}{2}}$ is only slightly larger than the absolute minimum obtained by varying α.

R_T and R_S (heated and salted above), for which Shir and Joseph show that a necessary *and* sufficient condition for the conduction solution to be the unique solution of $\mathscr{S}_t$ is $R_T < R_6$.

The next section discusses the nonlinear oscillatory motions and § 5 discusses the nonlinear monotonic motions. The relationship between these two equilibrium solutions is discussed in § 6.

4. The branch of oscillatory solutions

In the immediate neighbourhood of the oscillatory bifurcation point R_1, the nonlinear equilibrium solution can be obtained from a modified perturbation expansion of $\mathscr{S}_t$. For fixed R_S, this is achieved by introducing the new time variable

$$t' = pt \qquad (4.1)$$

and expanding each variable as

$$(\psi, T, S) = \sum_{n=1}^{\infty} \epsilon^n (\psi_n, T_n, S_n), \qquad (4.2\,a\text{–}c)$$

$$R_T = \sum_{n=0}^{\infty} \epsilon^n r_n \qquad (4.2\,d)$$

and

$$p = \sum_{n=0}^{\infty} \epsilon^n p_n, \qquad (4.2\,e)$$

where ϵ is a convenient expansion parameter whose value can be determined from $(4.2d)$ for given R_T. Substituting (4.1) and (4.2) into $\mathscr{S}_t$ and equating like powers of ϵ, we find that

$$\left.\begin{array}{l} \psi_1 \\ T_1 \\ S_1 \end{array}\right\} = -\pi\alpha \left\{\begin{array}{l} (k^2 + ip_0)^{-1} \\ (k^2 + ip_0)^{-1} \\ (\tau k^2 + ip_0)^{-1} \end{array}\right. \left.\begin{array}{l} \sin \pi\alpha x \\ \cos \pi\alpha x \\ \cos \pi\alpha x \end{array}\right\} e^{it'} \sin \pi z, \qquad \begin{array}{l}(4.3\,a)\\(4.3\,b)\\(4.3\,c)\end{array}$$

$$r_0 = R_1, \quad p_0 = p_0, \qquad (4.3\,d,e)$$

$$\psi_2 = 0, \qquad (4.4\,a)$$

$$T_2 = -\tfrac{1}{8}\pi^3\alpha^2 (k^2 + ip_0)^{-1} [\tfrac{1}{2}\pi^{-2} + (2\pi^2 + ip_0)^{-1} e^{2it'}] \sin 2\pi z, \qquad (4.4\,b)$$

$$S_2 = -\tfrac{1}{8}\pi^3\alpha^2 (\tau k^2 + ip_0)^{-1} [\tfrac{1}{2}\pi^{-2}\tau^{-1} + (2\pi^2\tau + ip_0)^{-1} e^{2it'}] \sin 2\pi z, \qquad (4.4\,c)$$

$$r_1 = 0, \quad p_1 = 0 \qquad (4.4\,d,e)$$

and that r_2 and p_2 are given by

$$\left\{ k^2 \frac{d}{dp_0} [(ip_0 + k^2)(ip_0 + \tau k^2)(i\sigma^{-1}p_0 + k^2)] - i\pi^2\alpha^2 (r_0 - R_S) \right\} p_2 - \pi^2\alpha^2 (ip_0 + \tau k^2) r_2$$

$$= \tfrac{1}{16}\pi^6\alpha^4 \{ [\pi^{-2}k^2(\tau^2 k^4 + p_0^2)^{-1} + (2\pi^2\tau + ip_0)^{-1}(\tau k^2 + ip_0)^{-1}] (ip_0 + k^2) R_S$$

$$- \pi^{-2}k^2 (k^4 + p_0^2)^{-1} + (2\pi^2 + ip_0)^{-1}(k^2 + ip_0)^{-1}] (ip_0 + \tau k^2) R_1 \}, \qquad (4.5)$$

where in (4.3), (4.4) and in similar equations to be presented below, the real part of each right-hand side represents the variable on the left. Using these results and the definitions (3.2) and (3.3), we find that as $R_T \to R_1$

$$N_T \sim 1 + \tfrac{1}{4}\pi^4\alpha^2 (k^2 + ip_0)^{-1} [\tfrac{1}{2}\pi^{-2} + (2\pi^2 + ip_0)^{-1} e^{2it'}] r_2^{-1}(R_T - R_1) \qquad (4.6)$$

and

$$N_S \sim 1 + \tfrac{1}{4}\pi^4\alpha^2 (\tau k^2 + ip_0)^{-1} [\tfrac{1}{2}\pi^{-2}\tau^{-1} + (2\pi^2\tau + ip_0)^{-1} e^{2it'}] r_2^{-1}(R_T - R_1). \qquad (4.7)$$
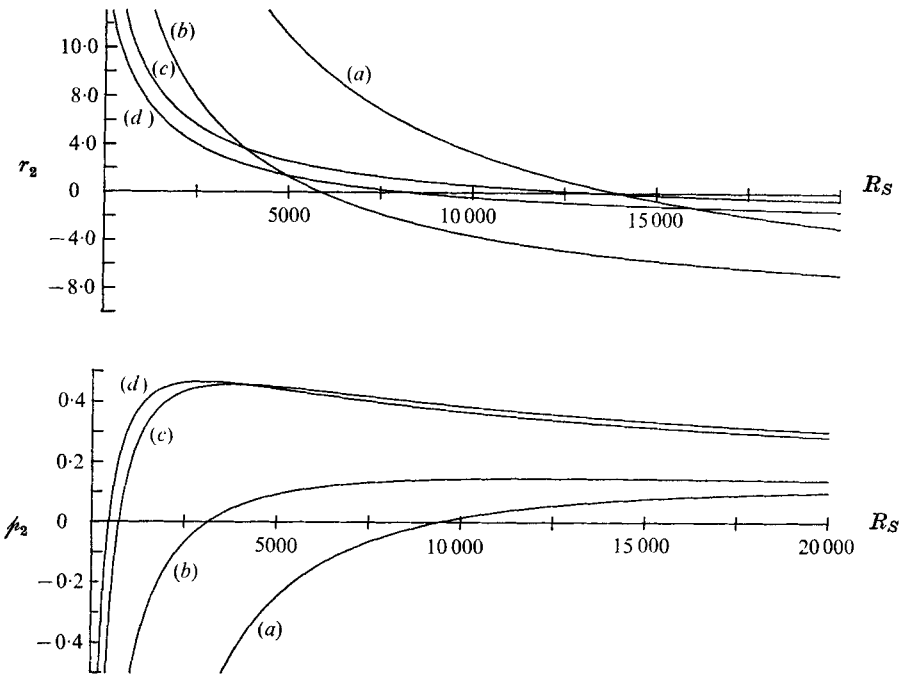
FIGURE 2. The solutions r_2 and μ_2 of (4.5) as a function of R_S for (a) $\sigma = 1$, $\tau = 10^{-\frac{1}{4}}$, (b) $\sigma = 1$, $\tau = 0\cdot1$, (c) $\sigma = 10$, $\tau = 0\cdot1$ and (d) $\sigma = 7$, $\tau = \frac{1}{80}$.
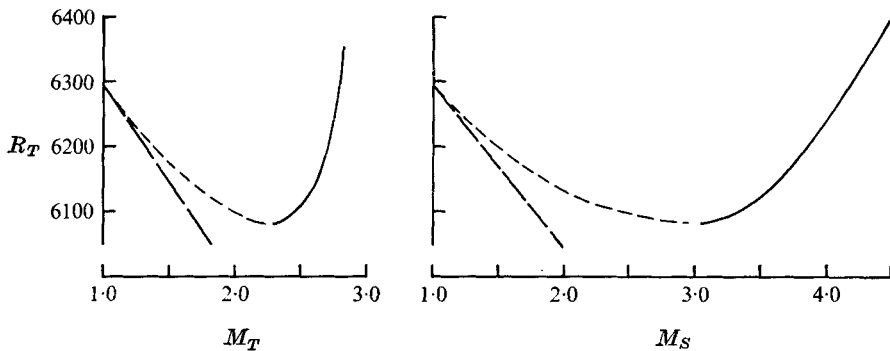

FIGURE 3. The oscillatory solution branch for $\sigma = 1$, $\tau = 0\cdot1$ and $R_S = 10^4$. ——, calculated stable portion of the branch; – – –, sketched unstable portion of the branch; —— ——, first approximation to the unstable portion, as obtained from (4.6) and (4.7).

Graphs of r_2 and μ_2 as functions of R_S for four values of σ and τ are displayed in figure 2 and the maximum value of N_S, obtained from the right-hand side of (4.7), is displayed in figures 3 and 5 for different values of σ, τ and R_S.

For small R_S, r_2 is positive. Thus R_T increases with amplitude (M_T or M_S) and the bifurcation point is supercritical. It can be shown in general (see for example Sattinger 1973) that, since they arise from a supercritical bifurcation, solutions on this branch will be stable with respect to any further linear two-

dimensional disturbance. The essence of this result can be explained by consideration of the associated potential energy function, for which all extrema represent equilibrium points, with potential energy minima (maxima) corresponding to stable (unstable) asymptotic solutions. For R_T larger than the value at a supercritical bifurcation point, the asymptotic solution of zero amplitude is unstable and hence is at a potential energy maximum. With increasing amplitude, the next equilibrium point is at a potential energy minimum and hence corresponds to a stable asymptotic solution. The numerical solution of $\mathscr{S}_t$ for small R_S confirmed this stability and the comparison between (4.6) and (4.7) and the numerical results is seen from figure 5 to be very good for quite a range of $R_T - R_1$. For large R_S, r_2 is negative and the bifurcation is thus subcritical. Solutions on subcritical branches are unstable because the zero-amplitude solution, being stable, is at a potential energy minimum and hence the next equilibrium point is at a potential energy maximum. Unstable solutions cannot be obtained from the scheme we have employed for the numerical solution of $\mathscr{S}_t$. However, it can be inferred from previous studies that the branch continues, and solutions on it are unstable, until a minimum value of R_T is reached. The branch then continues with the amplitude of the motion increasing with increasing R_T. The asymptotic solutions on this portion of the branch correspond to potential energy minima and the associated solutions are hence stable (and time dependent). An example of this behaviour is depicted in figure 3.

Comparisons of the period of the nonlinear motions obtained from $(4.2e)$, $(4.3e)$ and (4.5) and from the numerical solution of $\mathscr{S}_t$ are made in figure 4 for $\sigma = 1 \cdot 0$, $\tau = 10^{-\frac{1}{2}}$ and for three values of R_S. These three comparisons reflect the general tendency that for small values of R_S, carrying out the perturbation procedure to the order indicated (determining only $\not{p}_0$, $\not{p}_1$ and $\not{p}_2$) leads to results in good agreement with the exact solutions, while for larger values of R_S further terms are needed in order to obtain useful information.

For values of R_T beyond the range of applicability of the perturbation procedure, the numerical solution of $\mathscr{S}_t$ is needed to investigate the oscillatory branch further. A summary of the results of such an investigation is shown in figure 5 and table 3. The branch continues in the R_T, amplitude plane with the amplitude increasing with increasing R_T. Along this branch the period of the oscillation increases monotonically because of the increasing influence of the temperature field. Expressed in terms of the motion of a typical fluid particle, the explanation is that during its oscillatory displacement the particle experiences a restoring force which decreases as R_T increases, and hence the period increases. Figure 6 presents for one value of σ, τ, R_T and R_S a typical plot of N_T and N_S against time. The phase delay of N_S with respect to N_T is clearly seen. This delay occurs because the salt field diffuses more slowly than the temperature field. The slower diffusion of salt is also the reason why both the mean and the range of N_S are larger than those of N_T. Expressing N_S as a Fourier series and thus evaluating the power at each frequency, we obtain the result shown in figure 7 (a). This figure, which is to be viewed as an indication of the degree of nonlinearity of the motion, displays the large amount of power in the fundamental and the smaller, but by no means insignificant, power in the higher harmonics.
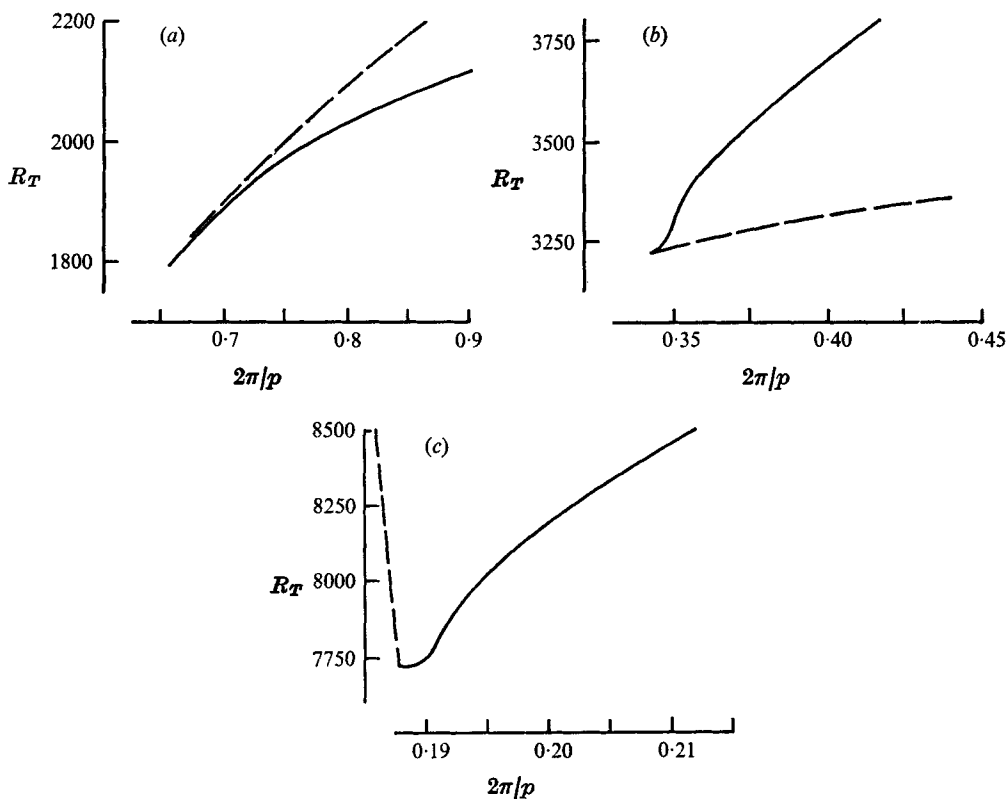
FIGURE 4. The period of oscillation $2\pi/p$ as a function of R_T for $\sigma = 1$, $\tau = 10^{-i}$ and (a) $R_S = 10^3$ ($R_1 = 1797$), (b) $R_S = 10^i$ ($R_1 = 3220$) and (c) $R_S = 10^4$ ($R_1 = 7720$). ———, result obtained from the numerical calculation of $\mathscr{S}_t$; — — —, result obtained from the modified perturbation expansion of §4.

Diagrams of the stream function, temperature, salinity and resulting density fields for one value of σ, τ and R_S are shown in figure 8. Eight representations of the fields, equally spaced in time and commencing when the maximum point of N_S is achieved, are presented which cover a complete cycle of N_T and N_S. The eight times are indicated in figure 6. The period of the basic fields is twice that of N_T and N_S and thus the figure presents these fields over only half a period. Their continuation occurs in the following manner: the ninth representation of the stream function field is the negative of the first in the depicted series, the tenth is the negative of the second and so on; and the ninth representations of the temperature, salinity and density fields are the reflexions about a vertical edge of the first representations, and so on.

Examining the stream function field first, we see that fluid particles move back and forth in their predominantly circular motion around part of the cell. The intensity of the motion reaches a maximum before the maximum of either N_T or N_S, which as explained above is the essential characteristic of oscillatory double-diffusive motion. At one point in this oscillation, rising hot fluid and sinking cold fluid produce the reflected S-shaped contours of the first representation
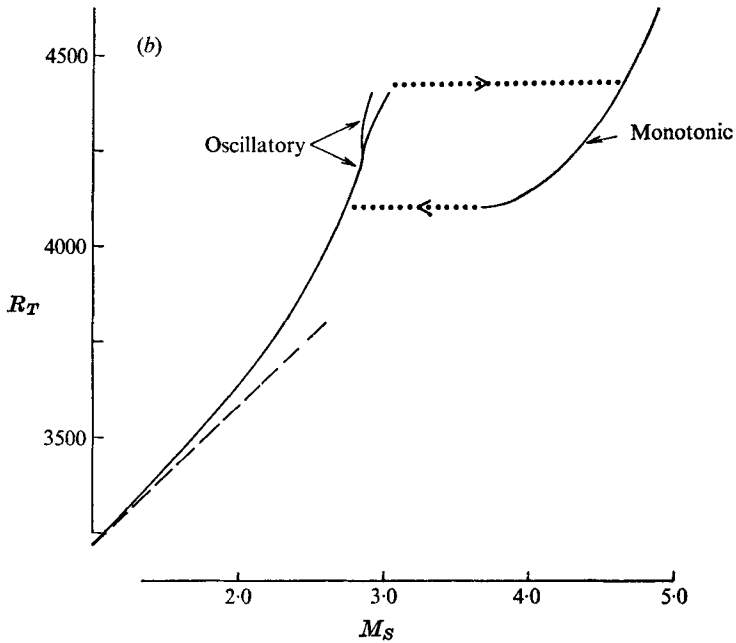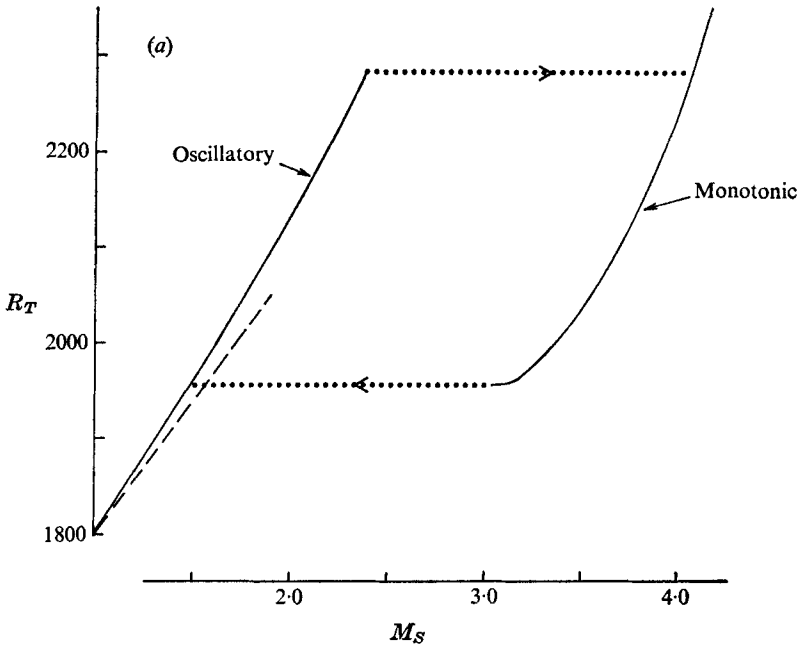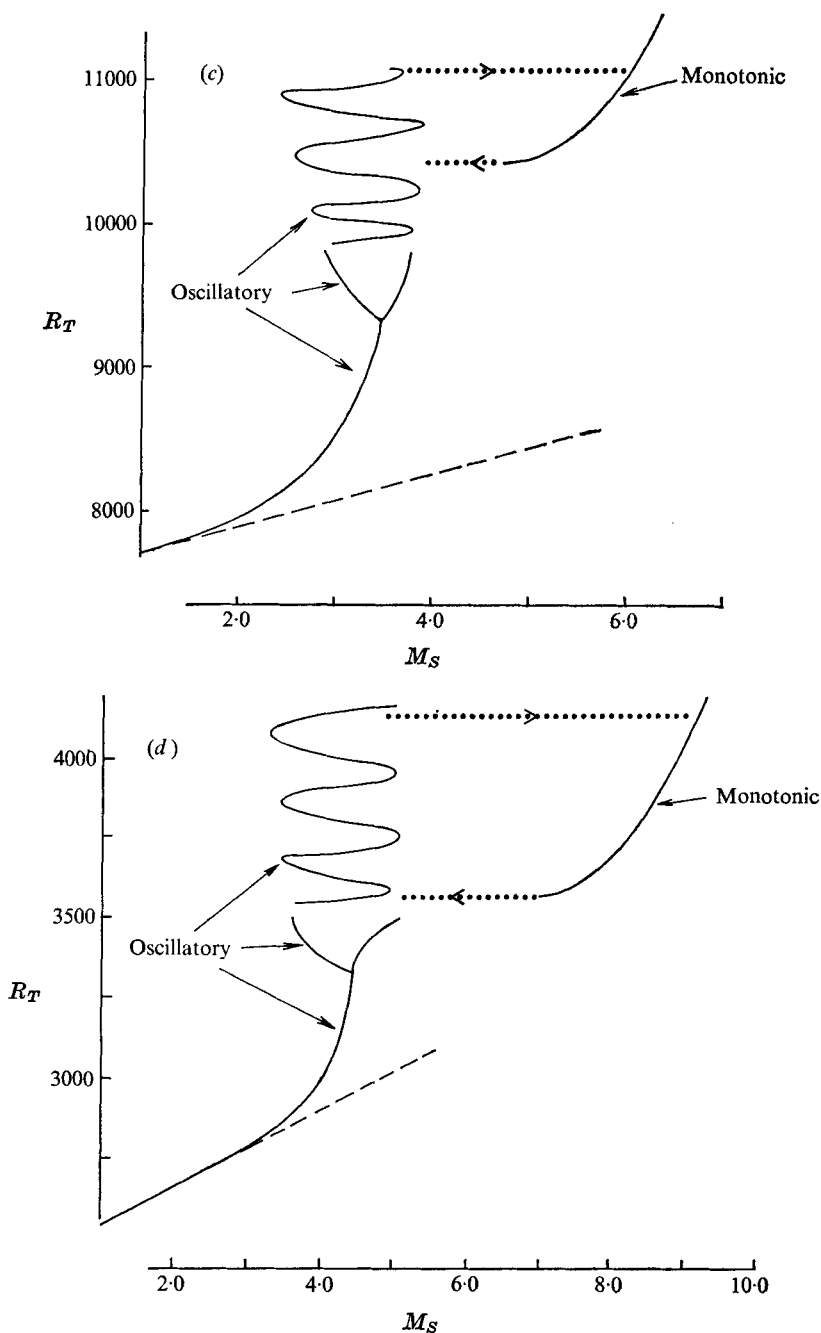
FIGURES 5(a,b). For caption see page 834.

FIGURE 5. The stable solution branches in an R_T, M_S plane for (a) $\sigma = 1, \tau = 10^{-i}, R_S = 10^3$, (b) $\sigma = 1, \tau = 10^{-i}, R_S = 10^i$, (c) $\sigma = 1, \tau = 10^{-i}, R_S = 10^4$ and (d) $\sigma = 1, \tau = 0\cdot1, R_S = 10^i$. For $R_2 < R_T < R_3$ both local maxima are shown and for $R_3 < R_T < R_4$ the rapidly oscillating curve indicates that no definite maximum can be assigned to the aperiodic motion in this range. The dots indicate the transitions that can take place between the oscillatory and monotonic branches. The dashed curve is the first approximation to the oscillatory solution branch, as obtained from (4.7).
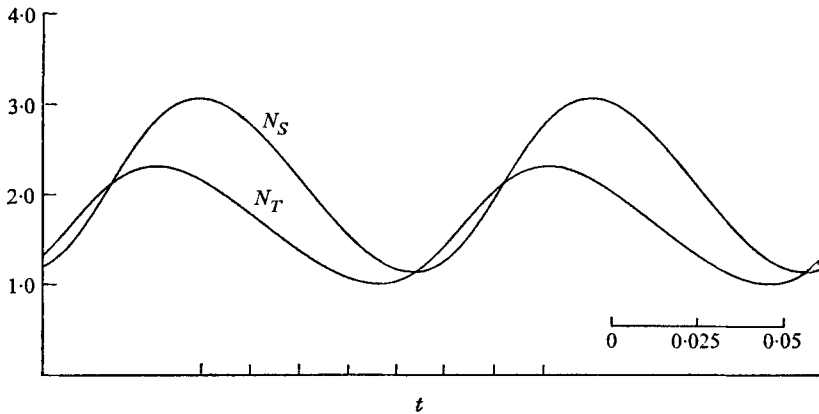
FIGURE 6. The thermal and saline Nusselt numbers as a function of time for
$$R_1 < R_T = 8600 < R_2, \quad R_S = 10^4, \quad \sigma = 1 \quad \text{and} \quad \tau = 10^{-\frac{1}{2}}.$$
The marks on the time axis indicate the times at which the stream function, temperature, salinity and density fields are displayed in figure 8. The horizontal line in the bottom right-hand corner represents 0·05 non-dimensional time units.
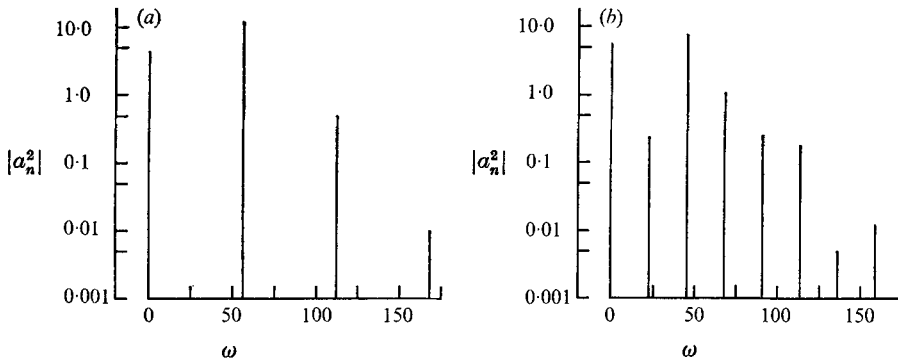

FIGURE 7. The spectral lines of $N_S(t)$ for $\sigma = 1$, $\tau = 10^{-\frac{1}{2}}$, $R_S = 10^4$ with (a) $R_1 < R_T = 8600 < R_2$ and (b) $R_2 < R_T = 9800 < R_3$.

of the temperature field. As the oscillation proceeds, the fluid reverses its direction and the temperature field relaxes, until in the fifth representation the horizontal temperature gradients are extremely small. In the last few representations, the horizontal temperature gradients increase until the temperature contours reach their maximum S-shape again. The salinity field is similar to the temperature field except for the following important differences. First, the salinity field attains its maximum structure after the temperature field, for the reason explained previously. Second, owing to the relatively slower diffusion of salt, the horizontal salinity gradients, which decrease to a large extent by diffusion, do so less rapidly than the horizontal temperature gradients. However, they increase approximately as rapidly because the increase occurs by the different process of advection, as evidenced by the increasing stream function field. Turning now to the density field, we clearly see the relative oscillations of the
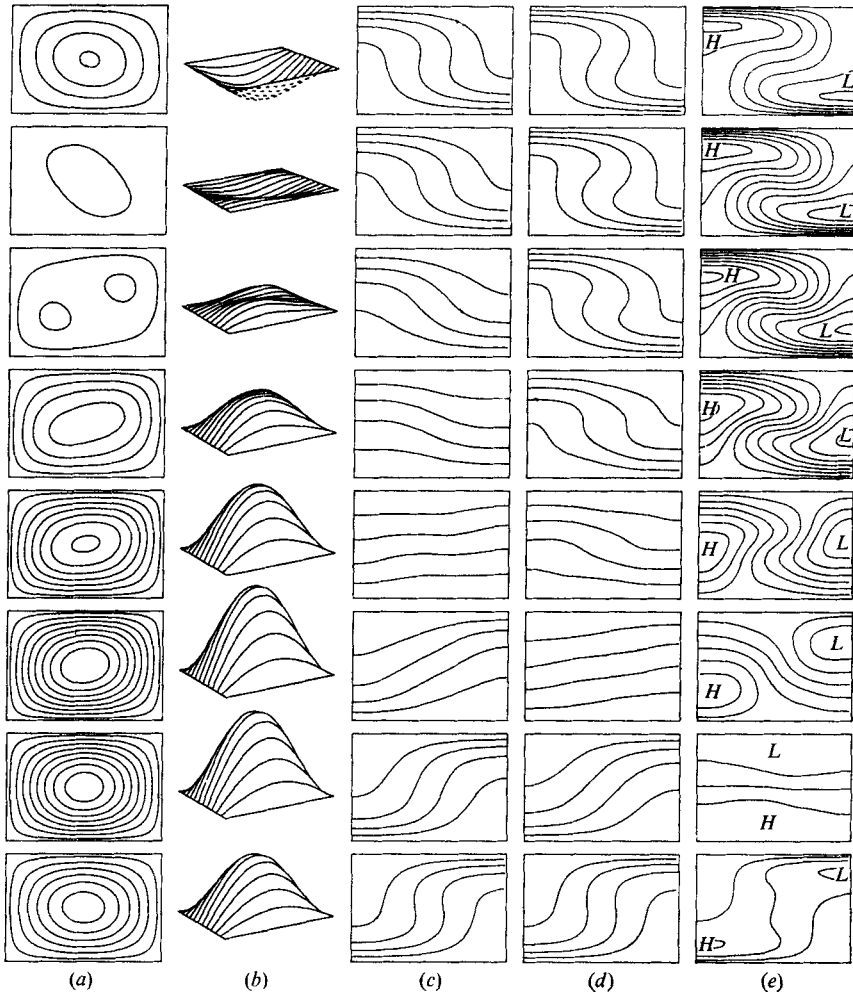
FIGURE 8. The basic fields for $R_T = 8600$, $R_S = 10^4$, $\sigma = 1$ and $\tau = 10^{-1}$. (a) The stream function ψ with a contour spacing of 0·0115. (b) Perspective representations of (a) viewed from a point 8 cell widths from the centre of the cell at an elevation of 0·3 rad from the horizontal plane and an azimuthal angle of 1·0 rad measured clockwise. (c) The non-dimensional temperature $T^*/\Delta T$ with a contour spacing of 0·2. (d) The non-dimensional salinity $S^*/\Delta S$ with a contour spacing of 0·2. (e) The non-dimensional density $\rho^*/\Delta\rho$, where $\Delta\rho$ is the density excess at the bottom of the cell over that at the top, with a contour spacing of 0·3. The H and L on the density representations indicate the regions of relatively heavy and light fluid.

heavy and light regions of the fluid. The comparison of the density field with the stream function field indicates the continual exchange that takes place between the potential energy and kinetic energy of the system. At one extreme, in the second representation, the stored potential energy is close to its maximum, with large regions of heavy fluid lying above relatively lighter fluid, and the kinetic energy is almost zero. Thereafter, the kinetic energy increases at the expense of the potential energy until at the other extreme, in the seventh representation,

$$R_T = R_1 = \frac{\sigma+\tau}{\sigma+1}R_S + \tfrac{27}{4}\pi^4(1+\tau)(1+\tau\sigma^{-1})$$

The lowest-mode linear instability point for oscillatory motion (overstability)

$$R_T = R_2$$

The transition point between motion with one maximum per period and that with two maxima per period

$$R_T = R_3$$

The transition point between motion with two maxima per period and aperiodic motion

$$R_T = R_4$$

The transition point between aperiodic motion and time-independent motion

$$R_T = R_4'$$

The maximum value of R_T for time-dependent motion

$$R_T = R_5$$

The minimum value of R_T for time-independent motion

$$R_T = R_6 = \tau^{-1}R_S + \tfrac{27}{4}\pi^4$$

The lowest-mode linear instability point for time-independent motion (exchange of stabilities)

$$R_T = R_{co} \text{ [equation (2.10)]}$$

The coalescence point of the two (complex-conjugate) eigenvalues of linear stability theory

$$R_T = R_1^{mn}$$
$$= \frac{\sigma+\tau}{\sigma+1}R_S + 2\pi^4 m^{-2}(n^2+\tfrac{1}{2}m^2)^3(1+\tau)(1+\tau\sigma^{-1})$$

The (m, n)-mode linear instability point for oscillatory motion

$$R_T = R_6^{mn} = \tau^{-1}R_S + 2\pi^4 m^{-2}(n^2+\tfrac{1}{2}m^2)^3$$

The (m, n)-mode linear instability point for time-independent motion

$$R_S = R_{1\cap 6} = \tfrac{27}{4}\pi^4\tau^2(1+\sigma^{-1})(1-\tau)^{-1}$$

The value of R_S at which $R_T = R_1$ intersects $R_T = R_6$

$$R_S = R_{bi} = \tfrac{27}{4}\pi^4\tau^2(\tau^{-1}-\tau)^{-1}$$

The value of R_S above (below) which the lowest exchange of stability point is a subcritical (supercritical) bifurcation

TABLE 1. Nomenclature

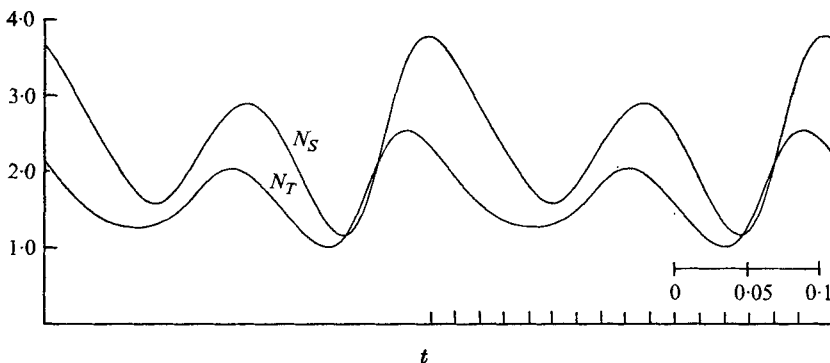FIGURE 9. The thermal and saline Nusselt numbers as a function of time for

$$R_2 < R_T = 9800 < R_3, \quad R_S = 10^4, \quad \sigma = 1 \quad \text{and} \quad \tau = 10^{-i}.$$

The marks on the time axis indicate the times at which the stream function, temperature, salinity and density fields are displayed in figure 10. The horizontal line in the bottom right-hand corner represents 0·1 non-dimensional time units.

$\sigma = 1{\cdot}0$, $\tau = 10^{-\frac{1}{2}}$, $R_S = 10^4$			$\sigma = 1{\cdot}0$, $\tau = 0{\cdot}1$, $R_S = 10^{\frac{5}{2}}$		
R_T		Period	R_T		Period
$7720(=R_1)$		$0{\cdot}0940$	$2535(=R_1)$		$0{\cdot}145$
7750		$0{\cdot}0949$	2600		$0{\cdot}146$
7800		$0{\cdot}0954$	2660		$0{\cdot}150$
8200		$0{\cdot}102$	2720		$0{\cdot}154$
8600		$0{\cdot}111$	2780		$0{\cdot}159$
9000		$0{\cdot}120$	3000		$0{\cdot}183$
9200		$0{\cdot}125$	3250		$0{\cdot}205$
9400	N_T	$0{\cdot}123$　$0{\cdot}134$	3325		$0{\cdot}212$
	N_S	$0{\cdot}126$　$0{\cdot}132$	3400	N_T	$0{\cdot}192$　$0{\cdot}236$
9600	N_T	$0{\cdot}122$　$0{\cdot}144$		N_S	$0{\cdot}209$　$0{\cdot}222$
	N_S	$0{\cdot}126$　$0{\cdot}140$	3500	N_T	$0{\cdot}189$　$0{\cdot}256$
9800	N_T	$0{\cdot}122$　$0{\cdot}155$		N_S	$0{\cdot}206$　$0{\cdot}239$
	N_S	$0{\cdot}126$　$0{\cdot}151$	3600–4100		Aperiodic
$10\,200$–1100		Aperiodic			

TABLE 2. The period of N_T and N_S. For $R_2 < R_T < R_3$ the time between the smaller maximum and the following larger maximum is given first followed by the time between the smaller maximum and the preceding larger maximum for N_T. The next line consists of these times for N_S.

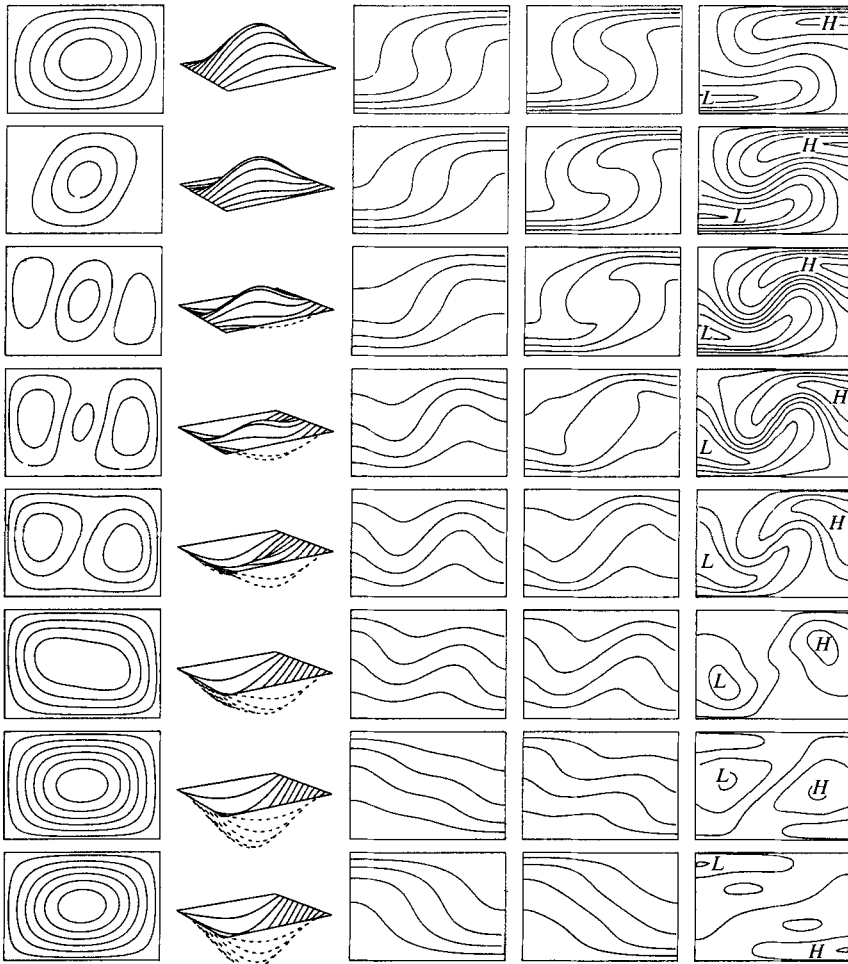

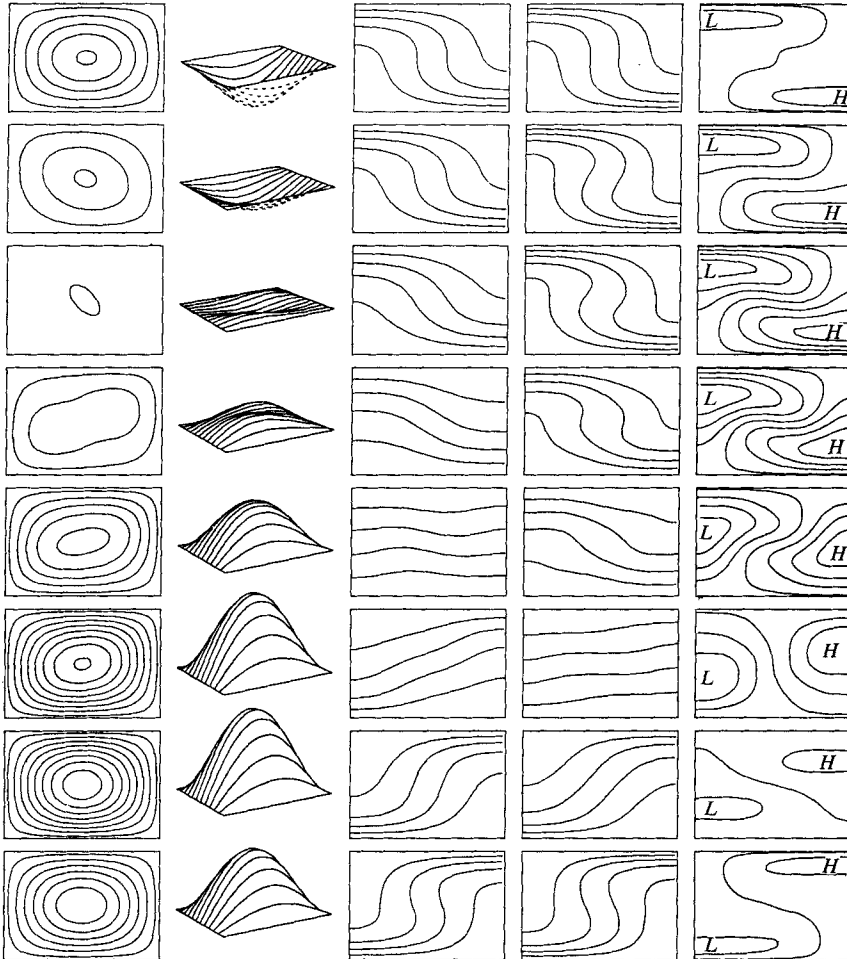FIGURE 10. For caption and remainder of figure see opposite page.

FIGURE 10. The basic fields as in figure 8 for $R_T = 9800$, $R_S = 10^4$, $\sigma = 1$, $\tau = 10^{-1}$. The contour spacing in the stream function representations is 0·0115, in the temperature and salinity representations 0·2 and in the density representations 3·0.

the stored potential energy is close to its minimum, with the density increasing with height everywhere, while the kinetic energy is close to its maximum.

As R_T increases, this form of motion continues until R_T reaches a specific value, R_2, say. At $R_T = R_2$ the motion changes in form. Either the motion becomes time independent, a situation discussed at the end of this section and in greater detail in the next section, or, the more general case, the motion develops a further structure as is indicated in the form of N_T or N_S as a function of time, as graphed in figure 9. In both N_T and N_S there are four extrema, two maxima and two minima, per period, where the period is defined in the usual sense as the time between two identical states. As seen in figure 9 and table 2 the time between the smaller maximum and the preceding larger maximum is greater than the

time between the smaller maximum and the following larger maximum. This holds for both N_T and N_S. As R_T increases above R_2 these times evolve continuously from the single period exhibited by N_T or N_S for R_T just below R_2. The power at each frequency of the Fourier representation of N_S is shown in figure 7 (b), from which it can be seen that this second form of motion has much more structure than the first form discussed previously.

The physical reason for this form of motion is that the increasing temperature difference attempts to induce monotonic motion. Fluid near one of the lower corners of the cell rises, sinks by a different route, rises by a smaller amount in an attempt to readjust the form of motion, sinks again and the total form of motion is then repeated. Other fluid particles in the cell move accordingly, as is shown in figure 10. This figure presents the stream function, temperature, salinity and density fields at sixteen equally spaced times over a complete cycle of N_T and N_S. The figure is constructed in a manner similar to figure 8 except that a complete cycle of N_T and N_S is now equal to a complete cycle in the motion fields rather than the previous half-cycle. The first representation is, as before, at the maximum of N_S and the times of each representation are indicated in figure 9.

The asymmetry of the two half-cycles is evident in all the fields, in contrast to the situation when $R_T < R_2$. Closely following the stream function field of maximum intensity (representation 15), the third, fourth and fifth representations of the stream function field show how part of the fluid moves with a predominantly vertical component through the interior portion of the cell. This motion is reflected in the corresponding density field, where heavy fluid descends just to the left of the middle of the cell and light fluid rises just to the right. The flow results in a temperature structure with an interior maximum and minimum (representations 4, 5 and 6) and a similar salinity field somewhat delayed (representations 5, 6 and 7). The first part of the cycle is thus very different from that with $R_T < R_2$, though the second part is quite similar, and almost all of the discussion of figure 8 applies to it. In terms of modern mathematical jargon, the solution for R_T less than R_2 is on a sphere, while for R_T greater than R_2 it is on a torus, and the transition at $R_T = R_2$ is called a bifurcating torus (Hirsch & Smale 1974). This form of motion occurs until $R_T = R_3$, say, at which value a transition either to a time-independent solution or, more generally, to a disordered, aperiodic form of motion occurs.

No stable asymptotic motion with three, four or more maxima per cycle was found, though it may be that such motion exists in a different parameter range from the one examined.

It is difficult to describe the aperiodic form of motion further. Figure 11 presents for one value of σ, τ, R_T and R_S a plot of N_T and N_S against time. Long computational runs have not revealed any periodic structure. It may be that the solutions are in some way similar to the apparently aperiodic solutions of a class of ordinary *difference* equations found by May (1976) to be made up of a finite number of periods. But, as discussed by May, the motion is so complicated that assigning a period to it is of very little use in understanding the motion or interpreting the results.

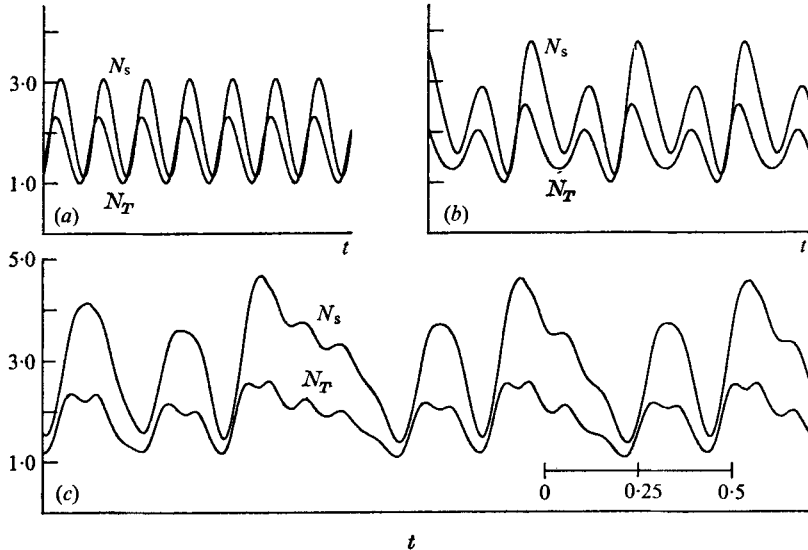Aperiodic motion continues to exist for increasing R_T until for $R_T = R_4$, say,

FIGURE 11. The thermal and saline Nusselt numbers as a function of time for $\sigma = 1, \tau = 10^{-\frac{1}{2}}$ and (a) $R_1 < R_T = 8600 < R_2$, (b) $R_2 < R_T = 9800 < R_3$ and (c) $R_3 < R_T = 11\,000 < R_4$. The horizontal line in the bottom right-hand corner of (c) represents 0·5 non-dimensional time units for each of the three graphs.

an asymptotic time-dependent solution can no longer be maintained and the only asymptotic solutions are time independent, a form of motion which will be analysed in the next section. For some values of σ, τ and R_S this time-independent form occurs before the solution passes through the two-maxima-per-cycle form of motion or the aperiodic form. Transitions which do occur are indicated in table 3. It is seen that for small values of R_S only the simplest form of time-dependent motion occurs, and that for large values of R_S the time-dependent branch includes the three different types of motion.

Also tabulated in table 3 are the linear oscillatory and monotonic critical Rayleigh numbers R_1^{21} and R_6^{21} for the second lowest mode. These Rayleigh numbers do not seem connected in any way with the Rayleigh numbers R_2, R_3 or R_4.

For future use we denote by R_4' the value of R_T at which the transition to an equilibrium time-independent solution occurs.

5. The branch of monotonic solutions

For all $R_T > R_4'$ monotonic motion ensues. As indicated in figure 12, such a form of motion exists in a double-diffusive fluid because the temperature field can produce an almost isosaline core, with all salinity gradients confined to boundary layers, which are thinner than the thermal boundary layers by an amount $\tau^{-\frac{1}{2}}$. In these salinity boundary layers, the effect of the stabilizing salinity gradient on the temperature field is small because of the different diffusivities. For sufficiently high R_T the destabilizing temperature effects can

R_S	R_1	R_2	R_3	R_4	R_5	R_6	R_1^{21}	R_6^{21}
				$\sigma = 1.0, \quad \tau = 10^{-4}, \quad R_{1n6} = 192\cdot3$				
10^3	1797	—	—	2275–2300	2000–2050	3820	2936	4477
$10^{3\cdot5}$	3220	4200–4300	—	4400–4500	4100–4150	10658	4359	11315
10^4	7720	9200–9400	9800–10200	11000–11200	10400–10500	32280	8859	32938
$1\cdot5 \times 10^4$	11010		<15000	15600–15800	15000–15200	48092	12150	48749
$2\cdot0 \times 10^4$	14301				19400–19600	63903	15440	64561
$2\cdot5 \times 10^4$	17592				24200–24400	79714	18731	80372
				$\sigma = 1.0, \quad \tau = 0.1, \quad R_{1n6} = 14\cdot6$				
10^3	1346	1750–1775	1775–1800	1900–2000	1700–1800	10658	2141	11315
$10^{3\cdot5}$	2535	3325–3400	3500–3600	4100–4200	3500–3600	32280	3330	32938
10^4	6296			<10200	8800–9000	100658	7091	101315
$1\cdot5 \times 10^4$	9046				12300–12700	150658	9841	151315
				$\sigma = 10.0, \quad \tau = 0.1, \quad R_{1n6} = 8\cdot0$				
10^3	1649			2100–2200	1700–1800	10658	2379	11315
$10^{3\cdot5}$	3634			4600–4800	3700–3800	32280	4365	32938
10^4	9912			9700–10000	9300–9600	100658	10643	101315
$1\cdot5 \times 10^4$	14503				13400–13700	150658	15233	151315

TABLE 3. The various transition points. A dash indicates that for that particular value of σ, τ and R_S no such transition occurs. A blank indicates that the value at which that specific transition takes place was not calculated.
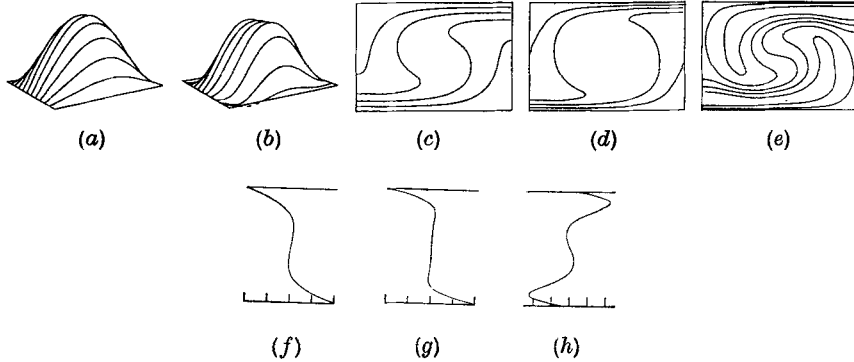
FIGURE 12. The basic fields for $R_T = 10\,700$, $R_S = 10^4$, $\sigma = 1$ and $\tau = 10^{-\frac{1}{2}}$. (a) The perspective representation of the stream function viewed from the same point P as in figure 8. (b) The perspective representation of the vorticity $\nabla^2 \psi$ viewed from P. (c), (d), (e) The non-dimensional temperature, salinity and density with contour spacings of 0·2, 0·2 and 1·0 respectively. (f) The mean temperature profile averaged across the cell. (g) The mean salinity profile. (h) The mean density profile.

thus overcome the restoring effects of the salinity. This steady form of motion is a very efficient way of transporting heat and salt and thus the equilibrium Nusselt numbers undergo a discontinuous increase as the solution changes from the oscillatory branch to the monotonic branch.

The fields displayed in figure 12 are typical of solutions on the monotonic branch. These all consist of steady, roughly circular motion with the largest vorticity in the central region of the cell. There is rising hot salty fluid adjacent to one edge of the cell and sinking relatively colder, fresher fluid adjacent to the other edge. The mean temperature and salinity gradients illustrate the thin, principally conductive, boundary layers and the larger, principally convective, interior, in which the mean gradients are very much smaller. The mean density gradient has a double structure in the boundary layer, due to the opposing influences of the temperature and salinity, and a much more uniform distribution in the interior.

As R_T increases above R'_4 the Nusselt numbers also increase. For very large R_T and fixed R_S, the temperature field and thermal Nusselt number are very similar to those for the purely thermal problem ($R_S = 0$) at the same R_T. Using the mean-field equations, Huppert (1972) suggests that at infinite Prandtl number

$$N_T = 0\cdot224\,[1 - (\tau^{\frac{1}{2}} R_S / R_T)]^{\frac{1}{3}}\, R_T^{\frac{1}{3}} \tag{5.1}$$

and

$$N_S = \tau^{-\frac{1}{2}} N_T \tag{5.2}$$

as $R_T \to \infty$. For a Prandtl number of 1·0, the multiplicative constant in (5.1) is increased, so that

$$N_T = 0\cdot238\,[1 - (\tau^{\frac{1}{2}} R_S / R_T)]^{\frac{1}{3}}\, R_T^{\frac{1}{3}} \quad (\sigma = 1, \quad R_T \to \infty). \tag{5.1'}$$

Nusselt numbers obtained from the numerical solution of $\mathscr{S}_t$ for $\sigma = 1$ are compared with those calculated from (5.1') and (5.2) in figure 13. It is seen that the agreement is rather good.
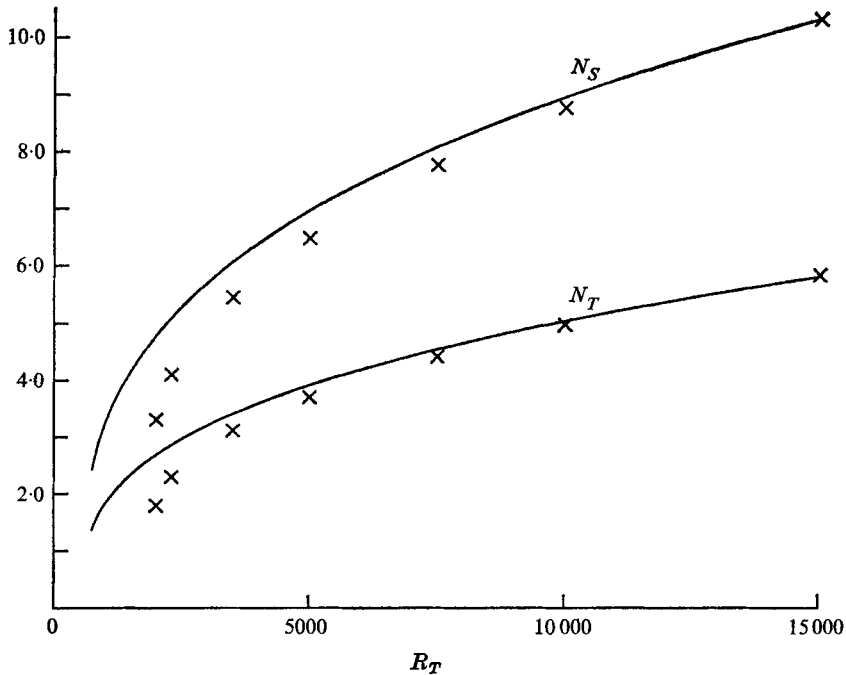
FIGURE 13. The thermal and saline Nusselt numbers as a function of R_T for $\sigma = 1$, $\tau = 10^{-1}$ and $R_S = 10^3$. The crosses are the results obtained from the numerical solution of $\mathscr{S}_t$ and the curves are the results (5.1') and (5.2) obtained from the mean-field calculations.

The accurate investigation by Moore & Weiss (1973) of the purely thermal problem indicates that an $R_T^{\frac{1}{3}}$ relationship between N_T and R_T holds for

$$5 < R/R_c < \sigma^{\frac{3}{2}},$$

where R_c is the linear critical Rayleigh number. At higher thermal Rayleigh numbers advection of vorticity becomes important and Moore & Weiss find that $N_T \propto R_T^{0.365}$. A large number of different results and a more complete discussion is contained in that paper and the reader is referred to it for further details.

As R_T is gradually decreased from some value greater than R_4', the equilibrium monotonic motions retrace the states that would have been obtained on increasing R_T from R_4'; thus there is a unique stable equilibrium solution to $\mathscr{S}_t$ for $R_T > R_4'$.

As R_T is decreased below R_4', an equilibrium monotonic solution continues to exist, with decreasing Nusselt numbers, until $R_T = R_5$, say. Further decrease in R_T leads to a solution on the oscillatory branch already described, or, if $R_5 < R_1$, to conduction. There is thus a hysteresis between these two different modes of motion, which will be discussed further in the next section.

It is entirely reasonable to suppose (but has not been rigorously proved) that the nonlinear steady branch emanates from the bifurcation point at $R_T = R_6$. The behaviour of the solution about $R_T = R_6$ can be obtained by using modified

perturbation theory in the same way as discussed in §3 except that all time derivatives are neglected. We find that: ψ, T and S are the same as (4.3a–c) if $\not{\mu}_0$ is set equal to zero and $e^{it'}$ is set equal to 1 therein; $r_0 = R_6$; ψ_2, T_2 and S_2 are the same as (4.4a–c) (with $\not{\mu}_0$ set equal to 0 and $e^{it'}$ to 1); and

$$r_2 = \tfrac{1}{8}\pi^2(R_6 - \tau^{-3}R_S)\,\alpha^2 k^{-2}. \tag{5.3}$$

Using these results and the definitions (3.3), (3.4) and (4.2), we find that

$$N_T \sim 1 + 2(R_6 - \tau^{-3}R_S)^{-1}(R_T - R_6) \quad (R_T \to R_6) \tag{5.4}$$

and

$$N_S \sim 1 + 2\tau^{-2}(R_6 - \tau^{-3}R_S)^{-1}(R_T - R_6) \quad (R_T \to R_6), \tag{5.5}$$

independent of α. The monotonic branch hence emanates from a subcritical bifurcation point ($r_2 < 0$) if

$$R_6 = \tau^{-1}R_S + \tfrac{27}{4}\pi^4 < \tau^{-3}R_S \tag{5.6a,b}$$

and from a supercritical bifurcation point otherwise. Rearranging (5.6b), we find that the bifurcation point is supercritical for $0 < R_S < R_{b1}$, say, and subcritical for $R_S > R_{b1}$, where

$$R_{b1} = \tfrac{27}{4}\pi^4\tau^2(\tau^{-1} - \tau)^{-1}. \tag{5.7}$$

By comparison of (5.7) with (2.9) it is apparent that

$$R_{b1} < R_{1\cap6}. \tag{5.8}$$

Hence, for that range of R_S for which linear theory predicts the onset of an oscillatory instability, the accompanying linear monotonic mode bifurcates subcritically.

Solutions on this subcritical branch are unstable to time-dependent two-dimensional disturbances until R_T attains a minimum value. The branch then continues, and solutions on it are stable, with the amplitude of the motion increasing as R_T increases. We identify this part of the branch as the one discussed at the beginning of the present section and displayed for four values of σ, τ and R_S in figure 5. We have not rigorously proved this identification but no other possibility seems at all plausible. A parabola of the form

$$R_T = a(N_S - N_{S,\min})^2 + R_5 \tag{5.9}$$

has been fitted through the three calculated cases on the monotonic branch with the lowest values of R_T (see table 6). The values of the saline Nusselt number at the minimum point, $N_{S,\min}$, are tabulated in table 4 for as many values of σ, τ and R_S for which it was believed that the curve fitting could be accurately carried out. The results of a similar procedure using the numerically obtained values of N_T are also tabulated in table 4. The two procedures lead to values of R_5 which differ by at most 1 %, a satisfactory amount considering that the procedure involves extrapolation.

The unstable portion of the monotonic branch of solutions might be approximated by

$$R_T = (R_6 - R_5)(N_{S,\min} - N_S)^2(N_{S,\min} - 1)^{-2} + R_5, \tag{5.10}$$

R_S	$N_{T,\,\min}$	$N_{S,\,\min}$	$R_5(T)$	$R_5(S)$
	$\sigma = 1\cdot0,\quad \tau = 10^{-\frac12}$			
10^3	1·64	3·07	2000	2000
$10^{\frac72}$	2·05	3·67	4110	4110
10^4	2·75	4·71	10450	10430
$1\cdot5 \times 10^4$	3·13	5·43	15060	15050
	$\sigma = 1\cdot0,\quad \tau = 0\cdot1$			
10^3	1·64	5·51	1740	1760
$10^{\frac72}$	2·26	6·94	3570	3570

TABLE 4. The minimum values of R_T and the corresponding thermal and saline Nusselt numbers for which monotonic convection can occur. These results are obtained by extrapolation of the three calculated solutions on the monotonic branch with the lowest value of R_T.

	$\sigma = 1\cdot0,\quad \tau = 10^{-\frac12}$			$\sigma = 1\cdot0,\quad \tau = 0\cdot1$	
R_S	$-dR_T/dN_S$	$-(dR_T/dN_S)_{\mathrm{par}}$	R_S	$-dR_T/dN_S$	$-(dR_T/dN_S)_{\mathrm{par}}$
10^3	1·4	1·7	10^3	4·9	3·9
$10^{\frac72}$	4·4	4·9	$10^{\frac72}$	16	9·7
10^4	14	12			
$1\cdot5 \times 1\cdot0^4$	21	15			

TABLE 5. The gradient in the R_T, N_S plane (of the unstable portion) of the monotonic branch at $R_T = R_6$. dR_T/dN_S is the gradient obtained by modified perturbation theory and $(dR_T/dN_S)_{\mathrm{par}}$ is that obtained from fitting a parabola through the minimum values of table 4 and the point $R_T = R_6$, $N_S = 1$.

a parabola which has a minimum of $R_T = R_5$ at $N_S = N_{S,\,\min}$ and passes through the point $R_T = R_6$, $N_S = 1$. The slope of this parabola at $N_S = 1$, $(dR_T/dN_S)_{\mathrm{par}}$ say, is given by

$$(dR_T/dN_S)_{\mathrm{par}} = -2(R_6 - R_5)(N_{S,\,\min} - 1)^{-1}. \qquad (5.11)$$

This is compared in table 5 with the value

$$dR_T/dN_S = \tfrac12\tau^2(R_6 - \tau^{-3}R_S), \qquad (5.12)$$

which is the correct slope of the steady branch at $N_S = 1$ as analytically determined by (5.5). Considering the simplicity of the parabolic representation (5.10) and the large differences between R_5 and R_6, we find the agreement between the two results to be quite good and conclude that (5.10) is a fair representation of the unstable portion of the monotonic branch.

6. The relationship between the branches of oscillatory and monotonic motion

As is clearly evident from figure 5 and table 2, the oscillatory and monotonic branches take quite different relative positions depending upon the values of σ, τ and R_S. The influence of these parameters can be summarized as follows. The linear steady mode is independent of σ because fluid particles undergoing steady linear motion conserve their momentum. Along the nonlinear part of the steady

branch the motion is only weakly dependent upon σ for the values of σ we are considering ($\sigma \geqslant 1$), just as in purely thermal convection (cf. Veronis 1966; Moore & Weiss 1973). By contrast, the motion on the oscillatory branch is quite dependent upon the value of σ because the magnitude of the phase lag between the temperature and displacement field, which drives the motion, is determined by σ. By way of contrast, the whole steady branch is strongly dependent on the magnitude of τ because its value indicates how slowly the salt field diffuses, and hence how effectively the salt field can overcome the tendency of the temperature field to drive steady convection. Along the oscillatory branch, on the other hand, the value of τ determines the phase lag between the salinity and temperature field, a lag which has only a small influence on the motion. The value of R_S, which indicates the magnitude of the stabilizing salt field, has a large influence on both branches.

Table 3 and the discussion in the last two sections summarize the various different orientations of the two branches and the hysteresis loop that connects them. Of particular interest is the value of R_5, the least thermal Rayleigh number for which (nonlinear) monotonic convection is possible. Table 3 presents upper and lower bounds to R_5 for various values of σ, τ and R_S. These are drawn on figure 14.

Consider first figure 14(a), which presents the bounds to R_5 for $\sigma = 1$, $\tau = 10^{-\frac{1}{2}}$, and six values of R_S. For the four lowest values of R_S, R_5 lies below R_{co} and above both R_S and R_1. For the two highest values of R_S, R_5 lies below R_S, but above R_1. An interesting observation, to be exploited further below, is that for all but the lowest value of R_S the four ranges within which R_5 lies can be joined by the straight line

$$R_T = 1200 + 0 \cdot 92 R_S \tag{6.1}$$

and this straight line only just passes beyond the range of R_5 when $R_S = 10^3$; (6.1) suggests $R_5 = 2120$ while the calculated range is 2000–2050.

Decreasing τ to 10^{-1} without altering σ, we obtain the results plotted in figure 14(b). The five ranges for R_S are, as expected, all less than those for $\tau = 10^{-1}$. For $R_S = 10^4$ and $R_S = 1 \cdot 5 \times 10^4$, R_5 is less than R_S. The straight line

$$R_T = 1043 + 0 \cdot 777 R_S \tag{6.2}$$

passes through the ranges calculated for R_5 for the three larger values of R_S but lies slightly above that calculated for $R_S = 10^3$; (6.2) suggests $R_5 = 1820$ while the calculated range is 1700–1800. No calculated value of R_5 is less than the linear oscillatory value R_1, and extrapolation of (6.2) beyond $R_S = 1 \cdot 5 \times 10^4$, an admittedly dangerous procedure, suggests that, for these values of σ and τ, there is no value of R_S for which $R_5 < R_1$. However, an appreciation of the different dependences of the position of the oscillatory branch and the steady branch on σ suggests that by increasing σ it may be possible to decrease R_S below R_1.

The ranges of R_5 for $\sigma = 10$ and $\tau = 10^{-1}$ are plotted in figure 14(c). For $R_S = 10^4$ or $1 \cdot 5 \times 10^4$, R_5 is less than both R_1 and R_S. Thus for these values of σ, τ and R_S, (nonlinear) monotonic convection can occur when the fluid is
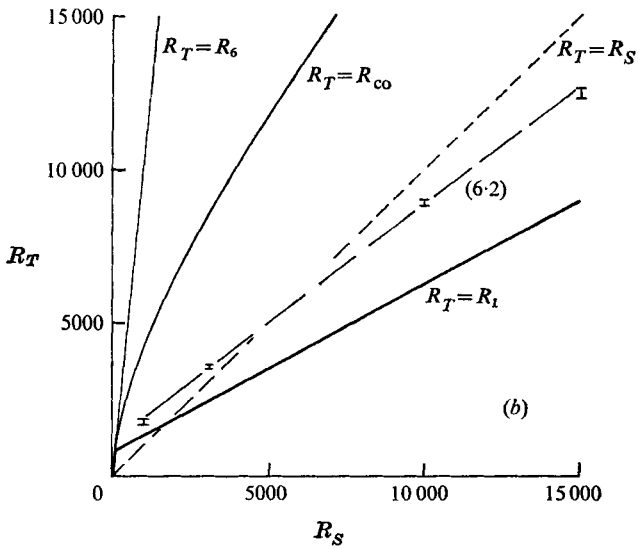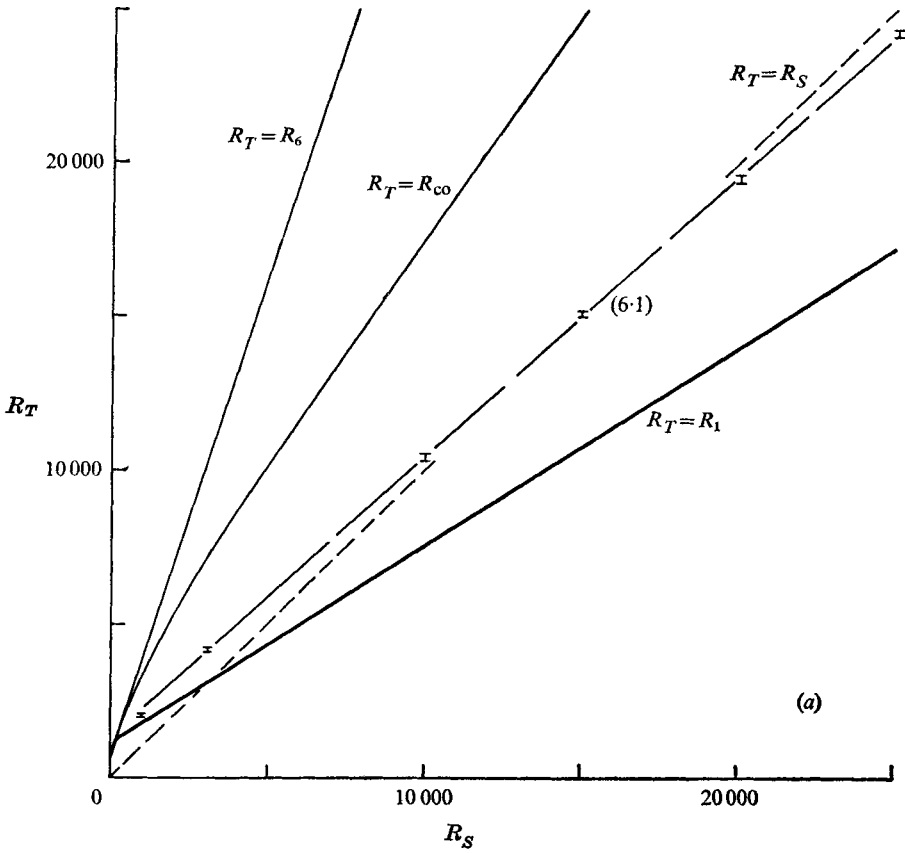
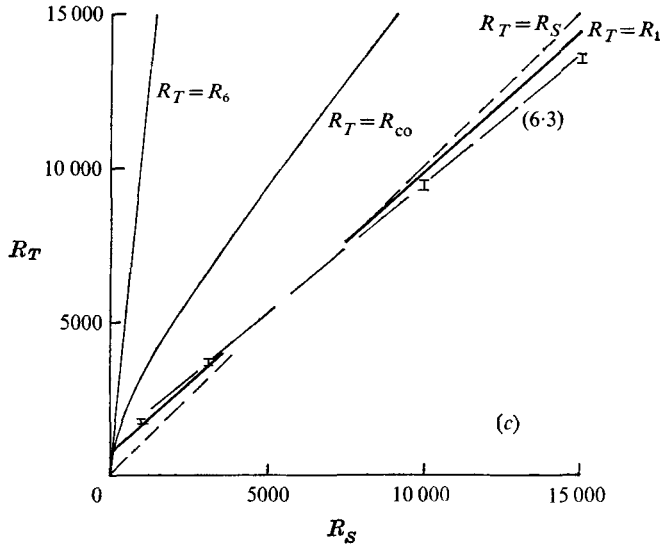FIGURES 14(*a*, *b*). For caption see opposite page.

FIGURE 14. The minimum value of R_T for which monotonic convection can occur for (a) $\sigma = 1, \tau = 10^{-\frac{1}{2}}$, (b) $\sigma = 1, \tau = 0\cdot1$ and (c) $\sigma = 10, \tau = 0\cdot1$. The vertical bars represent the regions within which the minimum occurs. The long-dashed straight lines (——) in (a), (b) and (c) are (6.1), (6.2) and (6.3) respectively.

statically stable and linear theory predicts the existence of only a conduction solution. As before, there is a straight line,

$$R_T = 1033 + 0\cdot844R_S, \tag{6.3}$$

which passes through the ranges of R_5 for the three larger values of R_S but lies slightly above that calculated for $R_S = 10^3$; (6.3) suggests $R_5 = 1877$, while the calculated range is 1700–1800.

7. Discussion and conclusions

Three-dimensional effects in the problem studied should be minimal for the following reason. In purely thermal convection between rigid boundaries, theoretical analysis indicates that two-dimensional rolls are stable to three-dimensional disturbances within a closed region of the R_T, α plane commonly referred to as the 'Busse balloon' (Busse 1967). Quite extensive experimental investigation has confirmed the existence and shape of the balloon (Busse & Whitehead 1971), and in particular the maximum value of $R_T = 22\,600$ for which very large Prandtl number two-dimensional rolls are stable. In contrast, theoretical analysis of purely thermal convection between *free* boundaries indicates that the balloon is still 'open' for infinite Prandtl number at $R_T = 20\,000$ (Straus 1972); that is, infinite Prandtl number two-dimensional rolls between free boundaries are stable up to at least $R_T = 20\,000$. It is commonly believed, and correctly in our opinion though no proof is yet available, that the Busse balloon for free boundaries remains open as R_T tends to infinity. Arguing by

analogy, we conjecture that the double-diffusive convective rolls between free boundaries treated herein are also stable to three-dimensional disturbances for all R_T.

The major conclusions of the work presented in this paper are as follows. Nonlinear asymptotic solutions of $\mathscr{S}_t$ belong to one of two branches. One is an oscillatory branch, which emanates from the linear oscillatory mode, either supercritically or, for sufficiently large values of R_S, subcritically. In general, as R_T is increased, the solution along this branch alters in such a way that the associated Nusselt numbers change from one maximum per period (figure 6), to two maxima per period (figure 9) to being aperiodic (figure 11). For sufficiently small R_S this branch does not exist at all. The other branch is composed of steady solutions, which emanate from the linear monotonic mode. Unless R_S is extremely small this bifurcation is subcritical. In this general (subcritical) case, solutions on the monotonic branch are unstable until the branch passes through its minimum value of R_T, whereafter the solutions are stable – at least in two dimensions. Stable solutions on both branches can exist at the same values of R_T, R_S, σ and τ. This leads to a hysteresis effect if solutions obtained from increasing and then decreasing R_T are followed. Depending upon the value of σ, τ and R_S, as R_T increases, instability may first occur as an oscillatory mode, either linear or nonlinear, or as a steady mode, either linear if R_S is very small or nonlinear otherwise. Thus nonlinear time-dependent double-diffusive convection can occur when linear stability theory indicates the existence of only a conduction solution, in contrast to the conjecture by Veronis (1968b). Finally, existence of an aperiodic solution which at a critical value of R_T becomes steady, by changing from one branch to another, indicates that by *increasing* R_T disordered motion can be suppressed.

While these conclusions hold exactly only for double-diffusive convection heated and salted from below, they act as a guide for a number of other problems. Amongst these are: convection in the presence of a magnetic field, currently being studied by N. O. Weiss (see Prigogine & Rice 1975, p. 101); convection in a rotating system, a preliminary study of which has been undertaken by Veronis (1968a); and convection accompanied by a strong Soret effect, whereby concentration gradients are induced by thermal gradients, as discussed in a number of papers in Prigogine & Rice (1975). The conclusions are *not* appropriate for double-diffusive convection heated and salted from above (salt-fingering), for which all asymptotic solutions are time independent.

Appendix. Numerical considerations

The numerical solutions of $\mathscr{S}_t$ were obtained by the methods described briefly in §3 and in detail by Moore *et al.* (1973), in which paper the parameters κ, κ_S, R' and ν are related to the parameters used in this paper by

$$\kappa = (\sigma R_T)^{-\frac{1}{2}}, \quad \kappa_S = \tau(\sigma R_T)^{-\frac{1}{2}}, \quad R' = R_S/R_T, \quad \nu = \sigma/R_T. \quad \text{(A 1 }a\text{–}d)$$

The majority of the calculations were performed by covering the region

$$0 \leqslant x \leqslant 1/\alpha, \quad 0 \leqslant z \leqslant \tfrac{1}{2}$$

with a uniform rectangular grid of points with N_x horizontal intervals and N_z vertical intervals. The solutions on the entire vertical interval $0 \leqslant z \leqslant 1$ were obtained, when required, by using the symmetry relationships

$$\psi(x,z) = \psi(1/\alpha - x, 1 - z), \quad \text{(A 2}a\text{)}$$

$$T(x,z) = -T(1/\alpha - x, 1 - z), \quad S(x,z) = -S(1/\alpha - x, 1 - z). \quad \text{(A 2}b,c\text{)}$$

If this symmetry exists at any particular time, Fourier analysis confirms that the solutions to (1.4)–(1.7) retain this symmetry for all future time (Veronis 1965). A large number of solutions were also calculated using a different program which obtained the solutions of $\mathscr{S}_t$ directly over the entire region $0 \leqslant x \leqslant 1/\alpha$, $0 \leqslant z \leqslant 1$. In each case the same solutions were obtained by the two different methods. The purpose of generally using the smaller size grid was that it halved both storage and computation time.

The time step δt was chosen both to yield an accurate solution to the DuFort–Frankel representation of the diffusion effects and to satisfy the Courant–Friedrichs–Lewy criterion for stable representation of the advection effects.

Accuracy in resolution was achieved by requiring at least three grid intervals across each feature. The method used to determine ψ from $\nabla^2\psi$ made it necessary for N_x to be 12, 24 or 48, though N_z could be any even number larger than or equal to 12. The most rapid spatial variation in each solution occurred in the horizontal salinity boundary layers on $z = 0, 1$. It was found that the requisite number of grid intervals were placed across these boundary layers if N_z was chosen to be at least three times N_S. An indication of the internal consistency of the numerical program is obtained from the fact that in monotonic asymptotic solutions the Nusselt numbers, calculated at the middle of each horizontal interval by adding the mean of the vertical convected flux across the top and bottom of the interval to the conducted flux across the interval, varied by less than 0·01 % across the entire layer.

Two additional tests on the accuracy of the program were performed. First, solutions obtained on a fine grid generally agreed to within 0·3 % with solutions obtained on a coarser grid with N_x and N_z half as large (but still sufficient for adequate resolution). Second, many of the solutions obtained by Veronis (1968*b*) were recomputed. The two sets of results differed by significantly less than the 1 % quoted by Veronis as the limit of accuracy of his solutions.

$\sigma = 1,\quad \tau = 10^{-\frac{1}{2}}$	$\sigma = 1,\quad \tau = 0\cdot1$	$\sigma = 10,\quad \tau = 0\cdot1$
	$R_S = 10^3$	
$N_x = 12,\quad N_z = 12$	$N_x = 12,\quad N_z = 12$	$N_x = 12,\quad N_z = 12$
(o) 1800 (50) 2000 2000 (100) 2200 2200 (25) 2275	(o) 1450 (50) 1750 (25) 1800 1900	(o) 1900
(m) 2050, 2100 (100) 2300 3500, 5000 (250) 15000		
	$N_x = 24,\quad N_z = 22$	$N_x = 24,\quad N_z = 18$
	(o) 1400, 1450 1700 (50) 1800, 1900	(o) 1600 (100) 2100
	(m) 1800 (100) 2100	(m) 1800, 2200
	$R_S = 10^{\frac{1}{2}}$	
$N_x = 12,\quad N_z = 14$	$N_x = 12,\quad N_z = 12$	$N_x = 24,\quad N_z = 28$
(o) 3250, 3300, 3500, 3800 4250, 4425 (25) 4475	(o) 2630 (30) 2780, 3000 3250, 3325, 3400	(o) 3500 (100) 4600
		(m) 3800 (100) 4000, 4800
$N_x = 24,\quad N_z = 20$	$N_x = 24,\quad N_z = 28$	
(o) 4100 (100) 4400	(o) 2600, 2630 3500 (100) 4100	
(m) 4150, 4200 (100) 4500	(m) 3600 (100) 4000, 4200	
	$R_S = 10^4$	
$N_x = 12,\quad N_z = 16$	$N_x = 12,\quad N_z = 12$	$N_x = 12,\quad N_z = 34$
(o) 7735, 7750 7800 (400) 10200 9200, 9300, 9600 10400 (100) 11000	(o) 6000 (50) 6100, 6175 6265, 6310, 6325, 6355	(o) 9000, 9300
(m) 10500 (100) 10700 11200, 11400		(m) 9600, 9900, 10000
	$N_x = 24,\quad N_z = 34$	$N_x = 24,\quad N_z = 34$
	(o) 8600 (200) 8800	(o) 9000 (200) 8400, 9500 9700
	(m) 9000, 9200, 10200	(m) 10000
	$R_S = 1\cdot5 \times 10^4$	
$N_x = 12,\quad N_z = 20$ $N_x = 24,\quad N_z = 20$	$N_x = 24,\quad N_z = 38$	$N_x = 12,\quad N_z = 38$
(o) 14800 (200) 15600	(o) 12300	(o) 13700
(m) 15200 (200) 15800	(m) 12700	(m) 14000
		$N_x = 24,\quad N_z = 38$
		(o) 12700 (300) 13600
		(m) 14400
		$N_x = 24,\quad N_z = 42$
		(o) 13400
		(m) 13700, 14000

$$R_S = 2 \times 10^4$$

$N_x = 24, \quad N_z = 24$

(*o*) 19400

(*m*) 19600 (200) 20000

$$R_S = 2 \cdot 5 \times 10^4$$

$N_x = 24, N_z = 24$

(*o*) 23600, 24000, 24200

(*m*) 24400

TABLE 6. Most of the computations carried out in this work. (*o*) indicates that the solution was oscillatory, (*m*) that it was monotonic.

On the IBM 370/165 at the University of Cambridge the time taken for 1000 time steps was approximately 20 s for $N_x = N_z = 12$. For each set of parameters the program was generally run for between 3000 and 10 000 steps, though some were run for as many as 40 000 steps. An indication of all the numerical experiments performed is given in table 6.

REFERENCES

BAINES, P. G. & GILL, A. E. 1969 On thermohaline convection with linear gradients. *J. Fluid Mech.* **37**, 289–306.

BUSSE, F. H. 1967 On the stability of two-dimensional convection in a layer heated from below. *J. Math. & Phys.* **46**, 140–143.

BUSSE, F. H. & WHITEHEAD, J. A. 1971 Instabilities of convection rolls in a high Prandtl number fluid. *J. Fluid Mech.* **47**, 305–20.

HIRSCH, M. W. & SMALE, S. 1974 *Differential Equations, Dynamical Systems, and Linear Algebra*. Academic.

HUPPERT, H. E. 1972 Double-diffusive convection. *Woods Hole Ocean. Inst. G.F.D. Notes*, no. 1, pp. 43–56.

HUPPERT, H. E. & MANINS, P. C. 1973 Limiting conditions for salt-fingering at an interface. *Deep-Sea Res.* **20**, 315–323.

MAY, R. M. 1976 Simple mathematical models with very complicated dynamics. *Nature*, **261**, 459–467.

MOORE, D. W. & SPIEGEL, E. A. 1966 A thermally excited non-linear oscillator. *Astrophys. J.* **143**, 871–887.

MOORE, D. R. & WEISS, N. O. 1973 Two-dimensional Rayleigh–Bénard convection. *J. Fluid Mech.* **58**, 289–312.

MOORE, D. R., PECKOVER, R. S. & WEISS, N. O. 1973 Difference methods for time-dependent two-dimensional convection. *Comp. Phys. Comm.* **6**, 198–220.

PRIGOGINE, I. & RICE, S. A. (ed.) 1975 *Adv. in Chem. Phys.* **32**.

SATTINGER, D. H. 1973 *Topics in Stability and Bifurcation Theory. Lecture Notes in Mathematics*, no. 309. Springer.

SHIR, C. C. & JOSEPH, D. D. 1968 Convective instability in a temperature and concentration field. *Arch. Rat. Mech. Anal.* **30**, 38–80.

SPIEGEL, E. A. 1971 Convection in stars. I. Basic Boussinesq convection. *Ann. Rev. Astron. Astrophys.* **9**, 323–352.

STERN, M. E. 1960 The 'salt-fountain' and thermohaline convection. *Tellus*, **12**, 172–175.

STOMMEL, H., ARONS, A. B. & BLANCHARD, D. 1956 An oceanographical curiosity: the perpetual salt fountain. *Deep-Sea Res.* **3**, 152–153.

STRAUS, J. M. 1972 Finite amplitude doubly diffusive convection. *J. Fluid Mech.* **56**, 353–374.

VERONIS, G. 1965 On finite amplitude instability in thermohaline convection. *J. Mar. Res.* **23**, 1–17.

VERONIS, G. 1966 Large-amplitude Bénard convection. *J. Fluid Mech.* **26**, 49–68.

VERONIS, G. 1968a Large-amplitude Bénard convection in a rotating fluid. *J. Fluid Mech.* **31**, 113–139.

VERONIS, G. 1968b Effect of a stabilizing gradient of solute on thermal convection. *J. Fluid Mech.* **34**, 315–336.